NATIONAL AERONAUTICS AND SPACE ADMINISTRATION

Technical Report No. 32-991

Average Properties of the Solar Wind as Determined by Mariner II

Marcia Neugebauer
Conway W. Snyder

JET PROPULSION LABORATORY
CALIFORNIA INSTITUTE OF TECHNOLOGY
PASADENA, CALIFORNIA

November 1, 1966

NATIONAL AERONAUTICS AND SPACE ADMINISTRATION

Technical Report No. 32-991

Average Properties of the Solar Wind as Determined by Mariner II

Marcia Neugebauer

Conway W. Snyder

Approved by:

R. J. Mackin, Jr., Manager
Physics Section

JET PROPULSION LABORATORY
CALIFORNIA INSTITUTE OF TECHNOLOGY
PASADENA, CALIFORNIA

November 1, 1966

Prepared Under Contract No. NAS 7-100
National Aeronautics & Space Administration

CONTENTS

I. Introduction 1

II. Trajectory of *Mariner II* and Solar Conditions 2

III. Instrumentation 2

IV. Method of Spectral Analysis 5

V. Results and Discussion 8

A. Velocity 8

B. Density 8

C. Temperature 11

D. The Definition of T_p 14

E. Nonthermal Ions 15

F. Alpha-Proton Ratio 17

G. Persistence of High-Velocity Streams 18

References 20

Appendix A. Method of Calculation of Plasma Parameters from Measured Spectra 23

Appendix B. Accuracy of Calculated Parameters 31

TABLES

1. **Summary of *Mariner II* trajectory** 3

2. ***E/Q*, proton velocity, and alpha-particle velocity corresponding to the center of each spectrometer channel** 4

3. **Time intervals for the *Mariner II* plasma spectrometer** 4

FIGURES

1. *Mariner II* positive-ion spectrometer 2
2. Block diagram of *Mariner II* positive-ion spectrometer 3
3. *Mariner II* electrostatic-analyzer transmission functions 4
4. Sample spectrum obtained by the *Mariner II* positive-ion spectrometer . 5
5. Three-hr average values of v and n_p (logarithmic scale) vs. time . . . 9
6. Twenty-seven-day averages of the daily averages of v, T_p, $3\theta_p/2$, and h vs. distance from the Sun 10
7. Daily average of n_pR^2 vs. the daily average of v 11
8. Twenty-seven-day averages of the daily averages of n_p, n_pv, and $v^2(M_pn_p + M_an_a)/2$ vs. distance from the Sun 12
9. Three-hr average values of v *and* T_p (logarithmic scale) vs. time 13
10. Daily-average value of the ratio of $3\theta_p/2$ vs. the daily-average solar-wind velocity 14
11. Three-hr averages of the high-energy-tail parameter h vs. the 3-hr averages of plasma flow velocity 16
12. Three consecutive positive-ion spectra obtained on October 7, 1962 . . 17
13. Three-hr value of N_a/N_h vs. the 3-hr average solar-wind velocity . . . 18
14. Daily-average alpha-proton density ratio n_a/n_p vs. daily-average solar-wind velocity for those days on which $N_a/N_h > 0.1$ 19
15. Mean values of n_a/n_p for each solar rotation vs. the logarithm of distance from the Sun 20

A-1. Contours of constant v and constant θ as a function of the currents in channels $m-1$, m, and $m+1$ for a single type of ion 24
A-2. The function $g(v)$ vs. v 25
A-3. Coordinate system used in data analysis 26
A-4. $f(\phi, s, \theta, v)$ vs. v as a function of θ for $\phi = 30°$ and $s = 0.0755$ 28
A-5. $f(\phi, s, \theta, v)$ vs. v as a function of s for $\phi = 30°$ and $\theta = 0.008$ 29
B-1. The largest possible fractional uncertainties in θ_p, n_p, and n_a/n_p arising from the 0.1-decade digitization of the current measurements . 31
B-2. Contours of constant v and constant θ as a function of the currents in channels $m-1$, m, and $m+1$ for an approximate and a square transmission function 32

ABSTRACT

This Report summarizes the properties of the positive-ion component of the solar wind observed during the four months of the *Mariner II* flight to and past Venus in 1962. The protons' average velocity and temperature were approximately 500 km/sec and 1.7×10^5 °K, respectively. Several streams of hot, high-velocity plasma were observed to recur at 27-day intervals, with peak velocity and temperature values of $\sim$ 830 km/sec and 9×10^5 °K. One of these streams existed for probably at least 18 months. Between streams, the velocity dropped to a low of 307 km/sec, while the temperature was $\sim 3 \times 10^4$ °K. Near 1 AU, the average density was approximately 5 protons/cm^3. The density was usually highest at the leading or western edge of each stream, with a maximum value of $\sim$ 80 protons/cm^3. Otherwise, the density varied inversely with the plasma velocity. The ions' velocity, temperature, and density were calculated from $\sim$ 35,000 energy/charge spectra by fitting the data to isotropic Maxwell-Boltzmann distributions in a reference frame moving away from the Sun at the solar-wind velocity. A model in which the protons and alpha particles have equal thermal velocities gives a better fit to the observed spectra than a model having equal temperatures. The spectra usually had high-energy tails, which became more pronounced at the higher plasma velocities. The velocity, temperature, and high-energy tail were not strongly dependent on distance from the Sun, whereas the density varied approximately as the inverse square of this distance.

I. INTRODUCTION

This Report is a summary of the average properties of the positive-ion component of the solar wind as determined by the electrostatic spectrometer on *Mariner II*.

Various plasma parameters such as velocity, density, and temperature have been calculated from the measured spectra and averaged over periods of either 3 hr (up to 49 complete spectra) or 24 hr. In later reports, these parameters will be related to properties of the interplanetary magnetic field on both a 3-hr or daily-average basis, and, for selected intervals, on as fine a time scale as the data allow.

II. TRAJECTORY OF *MARINER II* AND SOLAR CONDITIONS

Mariner II was launched on August 27, 1962, on a trajectory passing close to Venus. Usable data were obtained from the positive-ion spectrometer on board the spacecraft almost continuously from 1728 UT, August 29, through December 16, 1962; between 2015 UT, October 31, and 2132 UT, November 8, the scientific instruments on board were not operating. About 10 hr of data were obtained per day from December 17 through 1728 UT, December 30, when a failure occurred in a spacecraft reference-frequency circuit.

The *Mariner II* plasma data pertain to a period of declining solar activity during which no solar flare greater than class 2 was reported. The Zurich final relative sunspot numbers ranged from 0 to 88 with an average daily value of 36.3. Much of the geomagnetic activity for this period can be attributed to *M*-region storms. The geomagnetic indices K_p (3-hr) and A_p (daily) ranged from 0 to 7+ and 1 to 58, respectively, with the average daily A_p equal to 16 (Ref. 1).

Because the first plasma measurements were made when the spacecraft was 721,000 km from the Earth and the Sun–Earth–probe angle was 75.7 deg, no information on the properties of the Earth's magnetosphere or bow shock was obtained. The near-Venus observations were reported in an earlier paper (Ref. 2).

Table 1 summarizes the spacecraft trajectory. The orientation of the spacecraft was controlled by an attitude-stabilization system, which kept the entrance aperture of the spectrometer pointed to within 0.1 deg of the center of the Sun. During the first six days, the spacecraft slowly rolled about the Sun–probe line; thereafter, the Sun–probe–Earth plane remained fixed in the spacecraft.

III. INSTRUMENTATION

The configuration of the positive-ion spectrometer is shown in Fig. 1, and a block diagram is given in Fig. 2. The principal components of the spectrometer were (1) a cylindrical electrostatic analyzer, which separated positively charged ions according to their energy per unit charge (E/Q), (2) a programmer and a high-voltage sweep amplifier, which applied the proper balanced potentials to the plates of the analyzer, and (3) an electrometer, which measured the current from the charge collector at the output of the analyzer. The spectrometer was designed, built, and tested principally by C. Josias, J. L. Lawrence, Jr.[1], and H. R. Mertz at the Jet Propulsion Laboratory; it is described in greater detail in the Report by Josias and Lawrence (Ref. 3).

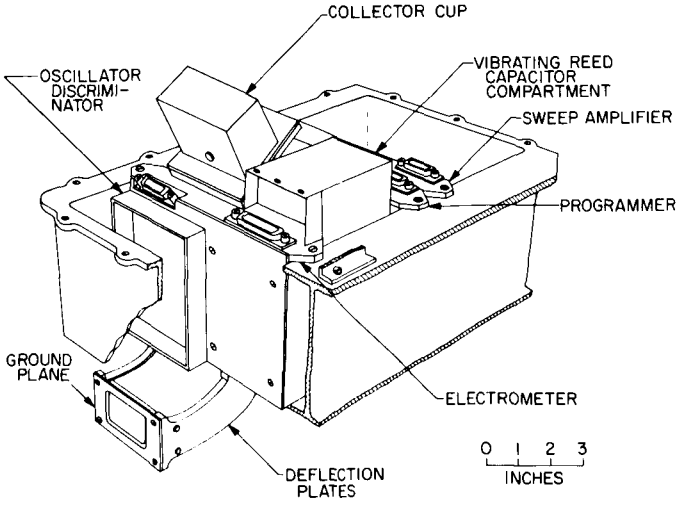

Fig. 1. *Mariner II* positive-ion spectrometer

The electrostatic analyzer was constructed of gold-plated magnesium; the interior was coated with gold black to minimize the amount of ultraviolet light that could enter the charge-collector region. The deflecting plates were 120 deg in length, and were separated by 1.3 cm. The entrance aperture was 5.0 cm^2 in area and rectangular in shape to provide approximately equal

[1]C. Josias is now President and J. L. Lawrence, Jr., Vice President of Analog Technology Corporation, Pasadena, California.

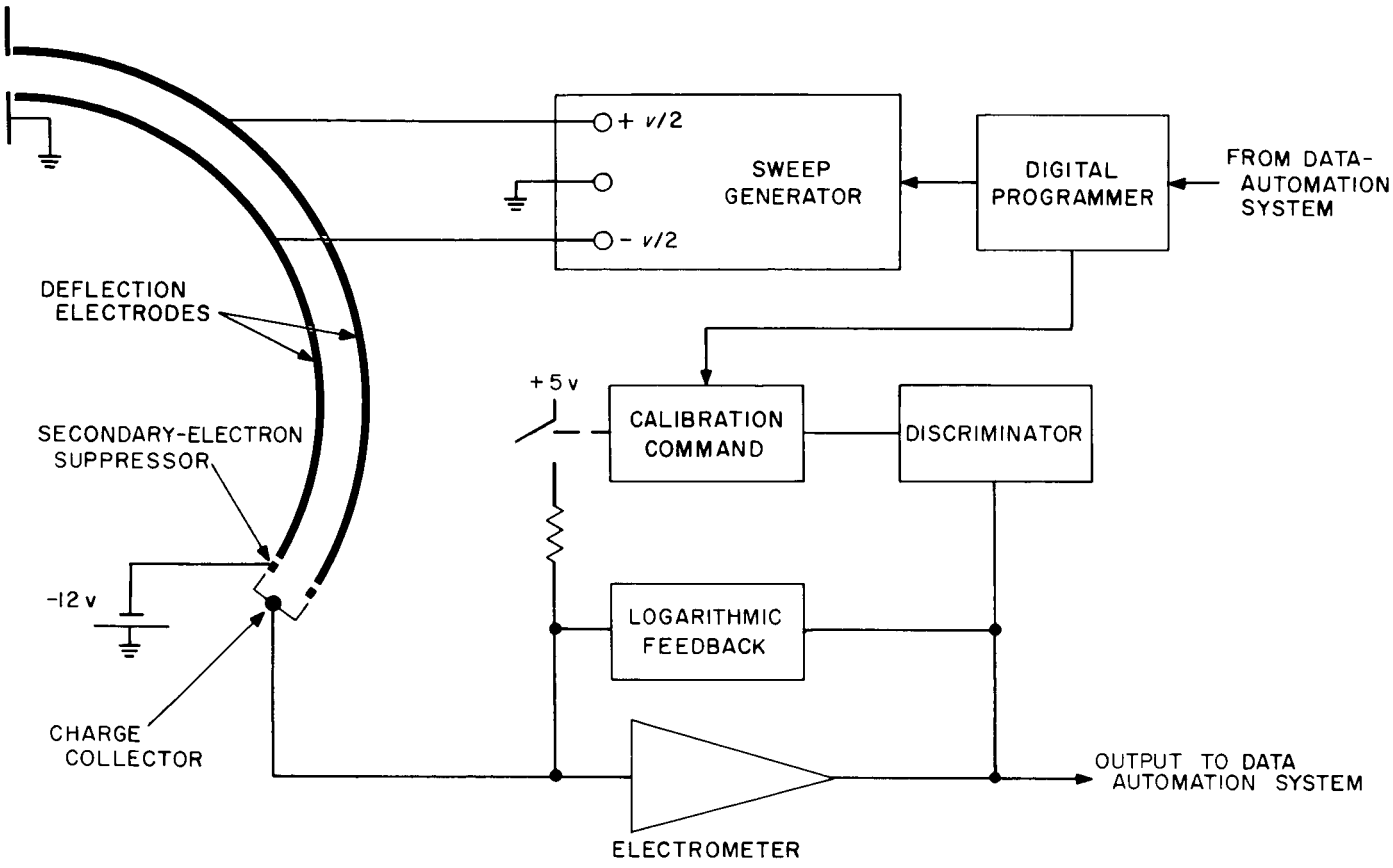

Fig. 2. Block diagram of *Mariner II* positive-ion spectrometer

Table 1. Summary of *Mariner II* trajectory

Date	Event	Distance from Sun, $\times 10^6$ km[a]	Solar latitude, deg[a]	Earth–Sun–probe angle, deg[a]	Sun–Earth–probe angle, deg	ϕ, roll angle, deg[b]	Tangential velocity, km/sec[a]	Radial velocity, km/sec[a]	Distance from Earth, $\times 10^6$ km[a]
August 29	First data	150.9	6.9	0.3	75.7	Rolling	26.6	−1.2	0.7
September 3	Attitude stabilized	150.3	7.4	0.7	72.4	17.4	26.8	−1.6	1.9
September 23	Start of solar rotation 1768	146.0	7.8	2.2	52.6	20.5	27.6	−3.4	6.9
October 7	Maximum Earth–Sun–probe angle	141.2	7.7	2.5	36.3	26.9	28.6	−4.5	10.5
October 20	Start of solar rotation 1769	135.6	7.0	2.1	20.6	40.6	29.7	−5.3	14.4
October 31	Earth overtaken	130.1	6.1	1.7	11.6	90.0	31.0	−6.0	18.8
November 16	Start of solar rotation 1770	121.6	4.1	4.4	19.3	26.4	33.2	−6.3	28.3
December 13	Start of solar rotation 1771	108.0	−1.4	18.5	37.4	4.8	37.8	−4.6	55.4
December 28	Perihelion	105.4	−4.0	30.2	43.4	3.0	40.0	0.0	77.1
December 30	Last data	105.5	−4.4	32.6	44.3	3.0	40.0	+0.7	81.7

[a]Presented graphically by Coleman, Ref. 4.

[b]The angle ϕ is defined in Section III; a related angle has been plotted by Coleman, Ref. 4.

angular acceptance for charged particles in two perpendicular planes. The theoretical angular and E/Q transmission functions in the plane of analysis (i.e., the fraction of a uniform beam of ions that reaches the collector as a function of energy and angle of incidence) are shown in Fig. 3.

The spectrometer was mounted on the spacecraft with the axis of the cylindrical deflecting plates parallel to the probe–Earth vector $\mathbf{R}_E$ (Fig. A-3, Appendix A). The angle ϕ, given in Table 1, is the angle between the vectors $\mathbf{R}_s \times \mathbf{v}_s$ and $\mathbf{R}_s \times \mathbf{R}_E$, where $\mathbf{R}_s$ is the probe–Sun vector, and $\mathbf{v}_s$ is the spacecraft velocity. This angle was very nearly equal to the angle between the Sun–probe–Earth plane and the ecliptic.

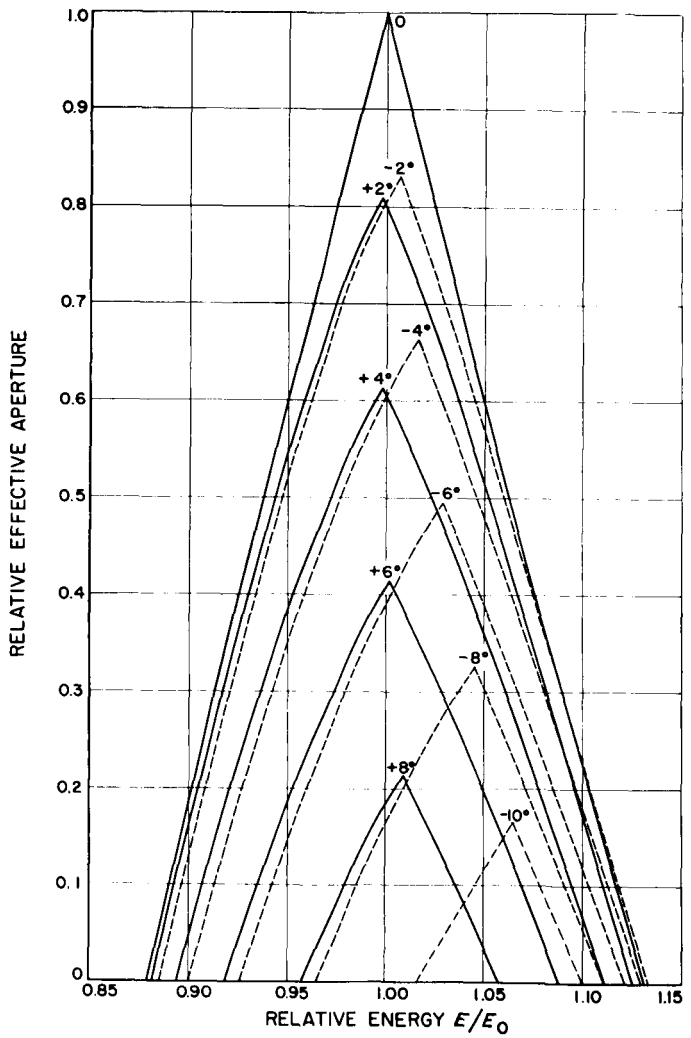

Fig. 3. *Mariner II* electrostatic-analyzer transmission functions

To obtain an E/Q spectrum of the solar-plasma ions, the deflecting voltage on the analyzer plates was changed by the programmer at intervals of about 18 sec in a sequence of ten ascending values. The voltages assumed for this analysis are given in Table 2. Laboratory measurements showed that the variation of these voltages with variations in instrument temperature amounted to $\pm$ 0.7% or less over the range $-$ 9 to + 68°C. Because a sensor in the instrument indicated temperatures between 29 and 77°C during the mission, no temperature corrections to the voltages were made.

Table 2. *E/Q*, proton velocity, and alpha-particle velocity corresponding to the center of each spectrometer channel

Channel	*E/Q*, v	Proton velocity, km/sec	Alpha velocity, km/sec
1	231	210	149
2	346	258	182
3	516	314	222
4	751	379	268
5	1124	464	328
6	1664	563	398
7	2476	690	488
8	3688	840	594
9	5508	1026	726
10	8224	1250	884

After 10 spectral measurements, a zero reading and a calibration reading (using a standard current of 10^{-10} amp) were taken with the plates connected together. The calibration permitted correction of the data for temperature variations in the electrometer, and for shifts in the analog-to-digital converter. The complete sequence of twelve measurements was repeated every 3.696 min.

Table 3. Time intervals for the *Mariner II* plasma spectrometer

Function	Time, sec
Time from start of one spectrum to start of the next	222
Average time to obtain a five-point spectrum	73
Average time between measurements in adjacent channels	18
Average time to obtain a single current measurement (peak)	~0.1

The electrometer, which utilized a dynamic-capacitor modulator to assure long-term stability, was capable of measuring currents from 10^{-6} to 10^{-13} amp, and its output was an accurately linear function of the logarithm of the input current over all but the lowest 1/2 decade of this 7-decade range (Ref. 3). The output dc voltage was converted by the spacecraft data-automation system into a digital reading with a quantization interval of 1/10 decade.

The electrometer time constant was a function of the magnitude of the measured current. At the 10^{-10} or 10^{-11} amp levels usually observed at the peak of a plasma spectrum, the relevant time constant was ~0.1 sec. The analog-to-digital conversion process, which occured about 18 sec after the change in plate voltage, required only about 1 msec (Ref. 3). Table 3 summarizes the several time intervals that were involved in this experiment.

IV. METHOD OF SPECTRAL ANALYSIS

Of the approximately 40,000 spectra telemetered to Earth from *Mariner*, 35,189 have been included in this analysis. All spectra for which any one of the 12 current readings was either missing or failed to pass a parity check have been omitted. Those spectra for which the current in any channel was several orders of magnitude different from both the preceding and the following several current measurements in that channel have also been omitted. Even if such an anomalous current measurement were correct, the calculated plasma properties probably would be incorrect because of the assumed time-independence of the spectrum. In general, the plasma spectra changed very slowly relative to the 3.7 min between successive spectra, for only about 10% of the current readings for a given channel changed by more than two digital steps from one spectrum to the next.

Many of the spectra were similar to that shown in Fig. 4, where the logarithm of the measured current is plotted against the channel number, or against the approximate logarithm of E/Q. The currents in the five other E/Q channels were very small and usually of negative polarity, the result, presumably, of electrons released from the suppressor electrode by the action of sunlight reflected down the deflection plates. This negative current was always below 10^{-13} amp, and frequently five to ten times smaller than this value for all energy channels. Because the peak positive-ion currents were usually in the range 10^{-10} to 10^{-11} amp, the positive-ion data have not been corrected for photoelectric effects.

If it is assumed that the positive-ion component of the solar plasma consisted of protons and alpha particles with isotropic Maxwell-Boltzmann distributions in a reference frame moving radially away from the Sun, then the peak of the alpha-particle distribution function would be at a value of E/Q equal to twice the value of E/Q at the proton peak, or approximately 1.74 spectrometer channels above the proton peak. Thus the left peak in each spectrum has been interpreted as a proton flux, and the right peak as a flux of alpha particles moving

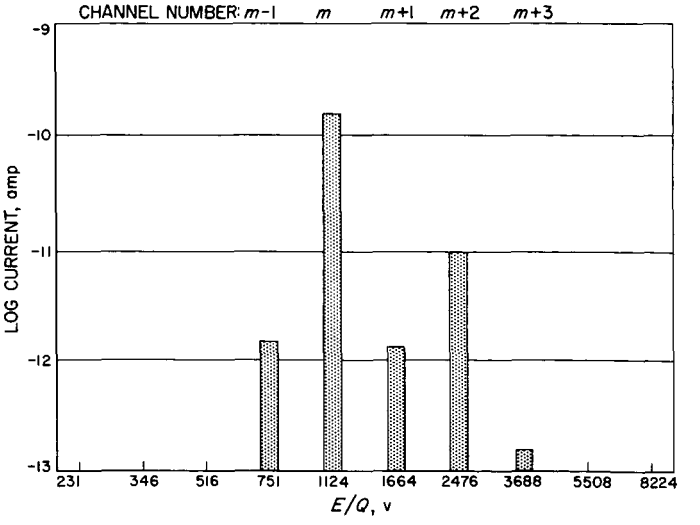

Fig. 4. Sample spectrum obtained by the *Mariner II* positive-ion spectrometer

with approximately the same bulk velocity as the protons. Equal bulk velocities for the two components should be assured by the influence of the fairly irregular interplanetary magnetic field.

A spectrum similar to that in Fig. 4 was analyzed as follows:

1. The currents in channels $m-1$, m (the "peak channel"), and $m+1$ were provisionally assumed to be due to protons only. By fitting a Maxwell-Boltzmann velocity distribution to these three measurements, the width of this proton peak and its location relative to the center of channel m were determined. The width determined the parameter

$$\theta_p \equiv 2kT_p/M_pv^2$$

where k is the Boltzmann constant, T_p is the proton temperature, M_p is the proton mass, and v is the plasma flow velocity.

2. This proton spectrum was then mathematically extended to channel $m+2$. The difference between the measured current in channel $m+2$ and this predicted proton current was assumed to be due to alpha particles.

3. The alpha-particle spectrum was determined from the alpha-particle current in channel $m+2$, and from the assumptions that the alpha particles and protons had equal flow velocities and appropriately related thermal-velocity distributions as discussed later.

4. An extension of the alpha-particle spectrum to channel $m+1$ gave the expected alpha-particle current in this channel.

5. After correction of the proton current in channel $m+1$, the calculations of steps one through four were repeated to obtain iterations of the proton spectrum until the iteration process either converged, or the calculated alpha-particle current in channel $m+1$ became greater than the total measured current in this channel. For this analysis, the final answer was considered to be known when the proton current in channel $m+1$ agreed with its value in the previous iteration within a factor of $10^{0.03} = 1.0715$, which corresponded to 0.3 of the instrument's digitization levels.

6. If a consistent set of proton and alpha-particle spectra could be obtained, the following plasma properties could be determined:

   a. The plasma bulk velocity v, which depends on the position of the proton peak relative to the center of channel m, on the value of θ_p (not a strong dependence), and on the velocity at the center of channel m (Table 2).

   b. The quantity T_p, which is determined by the values of θ_p and v. Although T_p is merely a measure of the velocity dispersion, it is convenient to define the term as "proton temperature."

   c. The proton and alpha-particle densities, n_p and n_a, which are determined by appropriate integrations over the final spectra.

   d. The parameter h, which is the logarithm of the ratio of the measured current to the predicted current in channel $m+3$, was calculated. The value of h is a measure of how well the assumed model fit the data.

Appendix A describes this spectral analysis procedure in more detail, and includes some of the mathematical shortcuts and approximations used in the actual analysis. Appendix B is a discussion of the uncertainties occurring in the calculated plasma parameters v, T_p, n_p, n_a/n_p, n_pmv^2, etc.

Of course, not all the measured spectra looked like Fig. 4. In general, any variation from this example could be classified in one or more of the following four categories:

1. With no current in channel $m+3$, there were four spectral points from which to calculate the four parameters v, T_p, n_p, and n_a for an assumed relationship between T_a and T_p. Because the parameter h could not be calculated, there was no way of telling how well any assumed model fit the data.

2. When channel $m+2$ had no current, higher channels had no current either. This type of spectrum might be expected when the composition changed to a state with relatively few alpha particles, when the apparent plasma density was so low that the currents in all channels were not as far above the sensitivity threshold as usual, when the alpha-particle peak fell midway between channels and, simultaneously, the alpha-particle temperature was relatively low, and when, if ever, the effective arrival direction of the alpha particles was at an appreciably greater angle to the Sun–probe line than were the protons. For these spectra, the proton velocity was calculated as usual. If the proton

peak was above the center of channel m, the proton temperature and density were then calculated. If, however, the proton peak was below the center of channel m, there may have been an appreciable alpha-particle contribution to the current in channel $m+1$; the values of n_p and T_p, therefore, were not calculated for that spectrum. Obviously, values could not be obtained for the parameters n_a and h.

3. If currents were observed in channel $m-2$ or in channel $m+4$, the extra values were not used in the analysis. Fewer than 1% of the observed spectra were of this type.

4. No current was observed in channel $m-1$, or no current was observed in channel $m+1$, if either n_p or θ_p was unusually low, or if the proton peak was quite far above the center of channel m so that channels m and $m+1$ had almost equal currents. In such cases, the upper limits of θ_p and T_p were obtained by assuming an actual current in the "missing" channel ($m-1$ or $m+1$) just at the electrometer's threshold of sensitivity; the spectral analysis then proceeded as outlined above. Lower limits for θ_p and T_p were obtained by assuming that n_p for this spectrum could not have been more than 3 standard deviations greater than the average n_p for a 15-hr period centered on the 3-hr period containing the spectrum in question. All spectra of this type were, of course, omitted from the calculation of the average n_p and its standard deviation. In addition to n_p, neither n_a nor h could be calculated for these spectra. The two values of v corresponding to the upper and lower limits of θ_p seldom differed by more than 2%. If there was no measurable current in either channel $m-1$ or channel $m+1$, the lower limits of θ_p and T_p were set equal to zero, and the velocity was assumed to equal the velocity at the center of channel m.

The spectral-analysis procedure described above and in Appendix A was applied to each of two models of the solar wind: (1) the equal-temperature model assumed that the protons and alpha particles were in thermodynamic equilibrium with each other (in the moving reference frame) at a temperature T; (2) the equal-thermal-velocity model assumed that the protons and alpha particles were separately in thermodynamic equilibrium, with the alpha-particle temperature T_a four times greater than the proton temperature T_p, giving the two types of ions identical, isotropic velocity distributions in the moving reference frame.

The analyses of the 35,189 spectra can be grouped as follows:

1. 12,473 spectra had unmeasurably small currents in either channel $m-1$, channel $m+1$, or both; therefore, only upper and lower limits were found for θ_p and T_p, while n_p, n_a, and h could not be calculated at all.

2. 13,263 spectra were successfully analyzed with the equal-thermal-velocity model of the solar wind to obtain v, θ_p (and therefore T_p), n_p, and n_a; there was also a measurable current in channel $m+3$ allowing the calculation of h. The equal-temperature model calculations converged for almost all of these spectra, but for only seven spectra did the equal-temperature model give a smaller absolute value of h than did the equal-thermal-velocity model. Apparently, then, the equal-thermal-velocity model better represents the state of the plasma than does the equal-temperature model.

3. 4,228 spectra were successfully analyzed with the equal-thermal-velocity model to obtain v, θ_p (and T_p), n_p, and n_a, but they did not have a current in channel $m+3$ large enough to permit the calculation of h. The results of the equal-thermal-velocity model for this group have been used for the data presentations in the rest of this paper.

4. 1,089 spectra were such that the analytical procedure did not converge for the equal-thermal-velocity model, and the results of the equal-temperature calculations are used in the data presentations that follow. Of these spectra, 884 had a measurable current in channel $m+3$, and h was calculated.

5. 4,136 spectra were such that neither model of the solar wind could be successfully applied, either because the calculations did not converge, or because there was no measurable current in channel $m+2$. If the proton peak for one of these spectra was above the center of channel m, the "proton-only" approximations for v, θ_p, T_p, and n_p were used. However, if the proton peak was below the center of channel m, the proton-only approximation for v was used, but this spectrum was not included in the average values of θ_p, T_p and n_p.

It is important to note in connection with groups 3 and 4 that the calculated values of v, θ_p, T_p and n_p are relatively insensitive to the choice of model. However, the width of the alpha-particle spectrum, and, therefore, the values of n_a and h, are strongly model-dependent.

V. RESULTS AND DISCUSSION

A. Velocity

The 3-hr averages of plasma velocity are shown in Fig. 5, where the time base was chosen to show the 27-day recurrence features associated with solar rotation. It is apparent that during this 4-month period the interplanetary plasma consisted of a series of long-lived, high-velocity streams separated by slower plasma. The 27-day recurrence pattern, the association of these streams with *M*-region geomagnetic storms, and the high correlation of the bulk velocity with the geomagnetic-activity indices K_p or A_p have been discussed in earlier papers (Refs. 5, 6, and 7). These conclusions still follow from the velocity profiles based on the more sophisticated calculations presented here.

While some of the high-velocity streams showed structures that were fairly symmetric, other observed velocity profiles were steeper on the leading or western edge than on the trailing edge (i.e., the velocity increased more rapidly than it decreased). Good examples of this behavior were observed in the streams with peak velocities observed on September 13, October 8, October 26, and November 21. This sort of profile is not unexpected for a reasonably symmetric source on the Sun (with the highest velocity at the center of the source), because the higher-velocity plasma tends to overtake the slower plasma ahead of it. At distances of 0.7 to 1.0 AU, however, the structure had not yet steepened into a shock front[2]. A high-velocity stream may eventually develop a shock front or a series of shocks at distances from the Sun appreciably greater than 1 AU.

The average daily-average velocity for the period August 29 through December 30, 1962, was 504 km/sec. The 3-hr averages ranged from 319 to 771 km/sec. The lowest and highest velocities sustained for at least three consecutive spectra occurred on November 18 when the velocity was between 306 and 308 km/sec for five spectra (18 min), and on December 20 when the velocity was between 815 and 842 km/sec for three spectra (11 min). From the velocity minima on November 13–14, November 18–20, November 28–29, December 7–8, and December 9–10, it would seem that the quiet, between-stream, solar-wind velocity was in the range 320 to $\sim$ 340 km/sec. Subsequent observations of solar-wind velocities as low as $\sim$ 250 km/sec by *IMP*, *OGO*, and *Vela* satellites[3], however, seem to contradict this conclusion. Perhaps the difference in minimum velocity reflects the difference in phase of the 11-yr solar cycle.

Scarf (Ref. 9) has calculated a quiet solar-wind velocity of 290 km/sec from a model in which there is uninhibited thermal conduction and viscous flow between 2 and 17 solar radii, followed by an adiabatic continuum flow region between 17 and 75 solar radii, with collisionless flow beyond 75 solar radii. Using a two-fluid model of the solar wind, Sturrock and Hartle (Ref. 10) calculated a velocity of 270 km/sec at 1 AU. These theoretically predicted velocities are not very different from the lowest observed velocities.

The averages of the plasma velocity over each solar-rotation period were also calculated in an attempt to separate the effect of variations in solar activity from the effect of Mariner's varying distance from the Sun. No clear radial variation of plasma velocity between 0.7 and 1.0 AU emerges from the calculations, as shown in Fig. 6. This result is consistent with theoretical predictions (Refs. 9, 11, 12, and 13). The basic inadequacy of the 27-day averaging method for determining the radial variations of plasma properties is apparent from Fig. 5; the high-velocity peaks were much less pronounced in the last half of solar rotation 1770 than in the four other rotations under consideration. The conclusion that plasma velocity is independent of radial variation comes as well from the constancy of the between-stream velocity minima noted above, which occurred at Sun–spacecraft distances between 0.824 and 0.732 AU.

B. Density

The number density of protons could be calculated for only 18,632 spectra, or 53% of the spectra for which velocity could be calculated. The resulting 3-hr and daily-average values of proton density and their relation to plasma velocity are shown in Figs. 5 and 7. It can be seen from Fig. 5 that the density generally reached a maximum on the leading edge of a high-velocity stream before maximum velocity was reached (September 12,

[2]The velocity change across the shock front observed on October 7 (Ref. 8) was from -370 to -450 km/sec, which was only a small fraction of the total velocity increase on October 7 and 8.

[3]Personal communication from H. S. Bridge, J. H. Wolfe, and I. Strong, 1966.

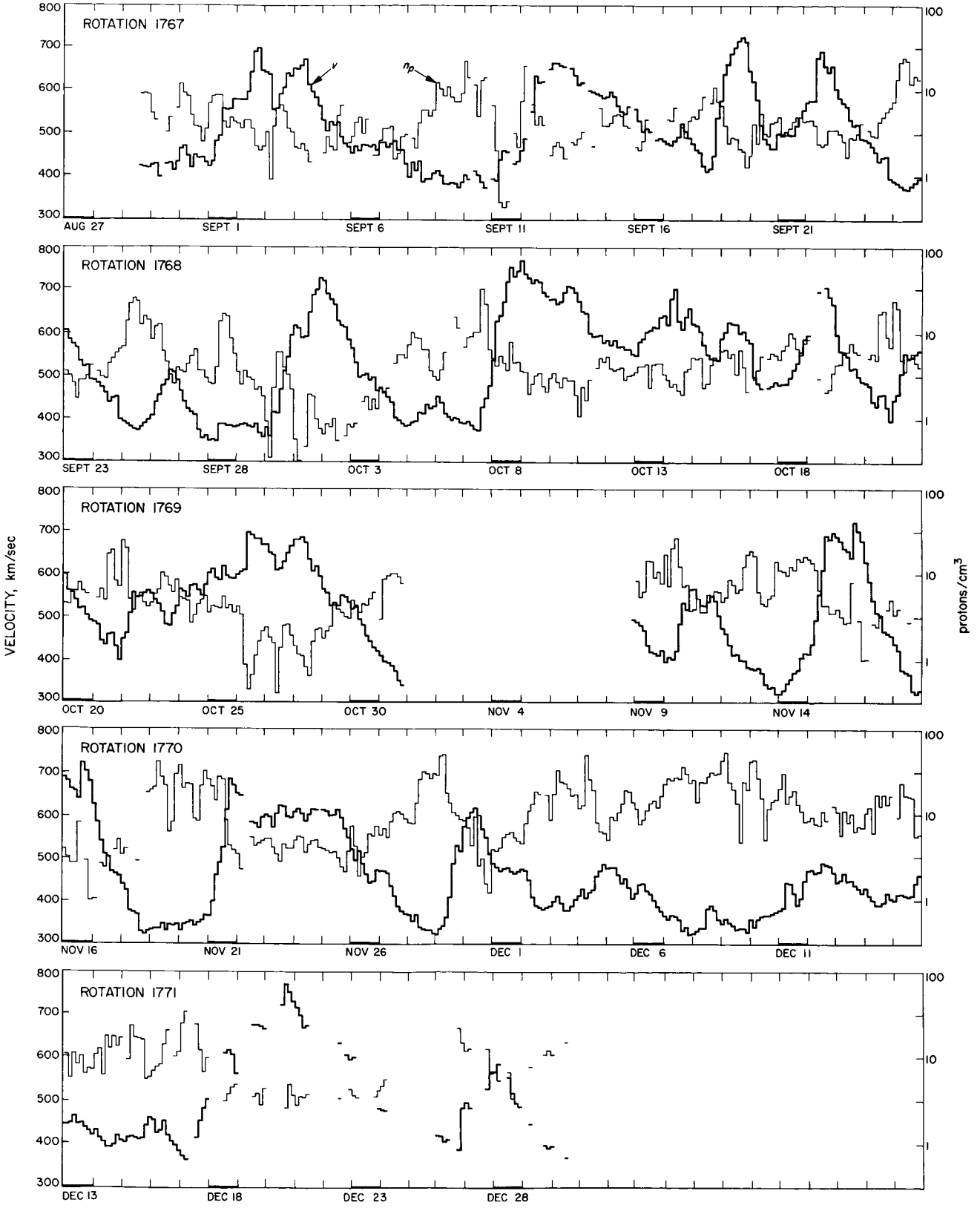

Fig. 5. Three-hr average values of v and n_p (logarithmic scale) vs. time

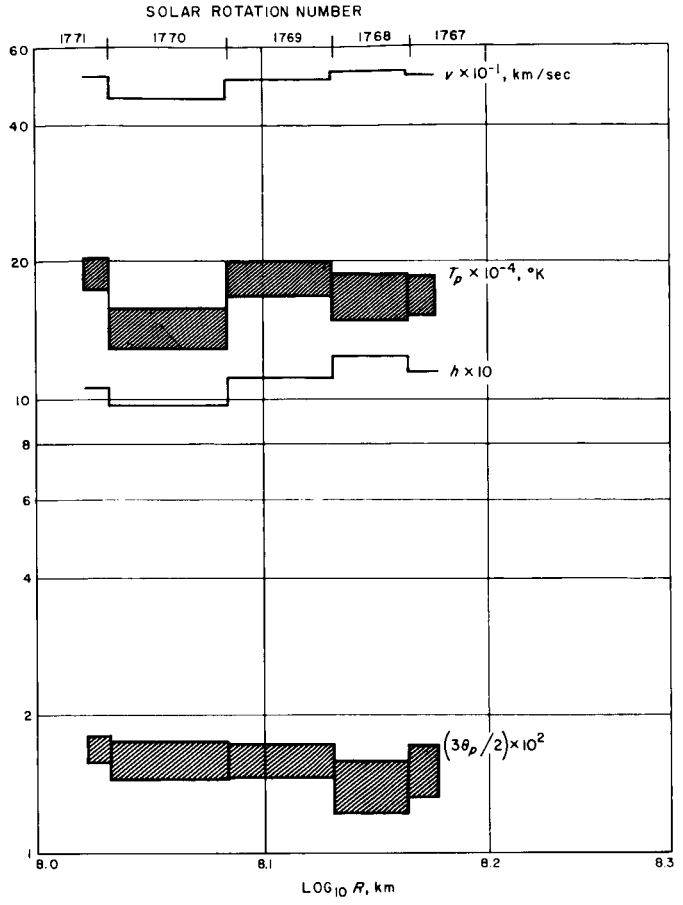

Fig. 6. Twenty-seven-day averages of the daily averages of v, T_p, $3\theta_p/2$, and h vs. distance from the Sun

September 30, October 7, November 10, and November 29 of Fig. 5 are good examples). The calculated density usually was very low (often less than 1 proton/cm^3) in the center of a high-velocity stream, as observed on September 4, September 13, September 19, October 2, October 26, October 28, and November 16.

The 3-hr average values of density ranged from 0.44 protons/cm^3 on September 11 to 54 protons/cm^3 on December 9. (In Fig. 5, there are four 3-hr intervals with n_p between 0.31 and 0.42 protons/cm^3, but each of these intervals contained only two or three spectra for which density could be calculated; the average values, then, were perhaps not representative.) The lowest density maintained for at least three consecutive spectra was observed on September 11 when there were between 0.081 and 0.094 protons/cm^3 for four spectra. The highest density was observed between high-velocity streams on December 9 when there were between 70 and 88 protons/cm^3 for three spectra.

It is also apparent from Fig. 5 that the proton density generally increased with time as *Mariner II* approached perihelion. Further analysis of this effect is based on Fig. 8, in which the 27-day averages of the daily averages of the proton density n_p, of the proton flux $n_p v$, and of the momentum flux, or energy density associated with the bulk motion v^2 $(M_p\, n_p + M_a\, n_a)/2$ are shown as a function of solar distance. The slopes for an inverse-square relation are also given in this figure. Despite the large effects of the varying nature of the high-velocity streams from one solar rotation to the next, the dependence of the plasma parameters on the inverse square of the distance from the Sun can perhaps be detected.

This inverse-square relation was used to normalize the daily-average values of proton density to 1 AU (Fig. 7). The average of the normalized daily averages for the four months of these observations was 5.4 protons/cm^3. Figure 7 also shows a rough inverse proportionality between the logarithm of the normalized density and the plasma velocity. Thus the density was much more variable than the velocity, and such parameters as mass flux, momentum flux, and energy flux were roughly correlated with density and showed little correlation with velocity or the K_p index.

For comparison with near-Earth observations, the average daily averages (not normalized) during solar rotation number 1767 when *Mariner II* was between 1.01 and 0.97 AU from the Sun were:

$$n_p = 5.0 \text{ protons/cm}^3$$

$$n_p v = 2.4 \times 10^8 \text{ protons/cm}^2 \text{ sec}$$

$$v^2(M_p\, n_p + M_a\, n_a)/2 = 1.2 \times 10^{-8} \text{ ergs/cm}^3$$

Both density and flux for the between-stream periods were consistently greater by factors between 2 and 6 than the values predicted by Scarf's (Ref. 9) quiet solar-wind model.

As discussed in Appendix A, the shapes of the measured spectra and, therefore, the calculated values of velocity and temperature were relatively insensitive to the plasma's angle of incidence. As seen in Fig. 3, however, the absolute values of the measured currents, and thus the calculated proton density depended strongly on the angle of incidence. The calculations presented here were based on the assumption of a radial velocity corrected for aberration due to the spacecraft's motion. The

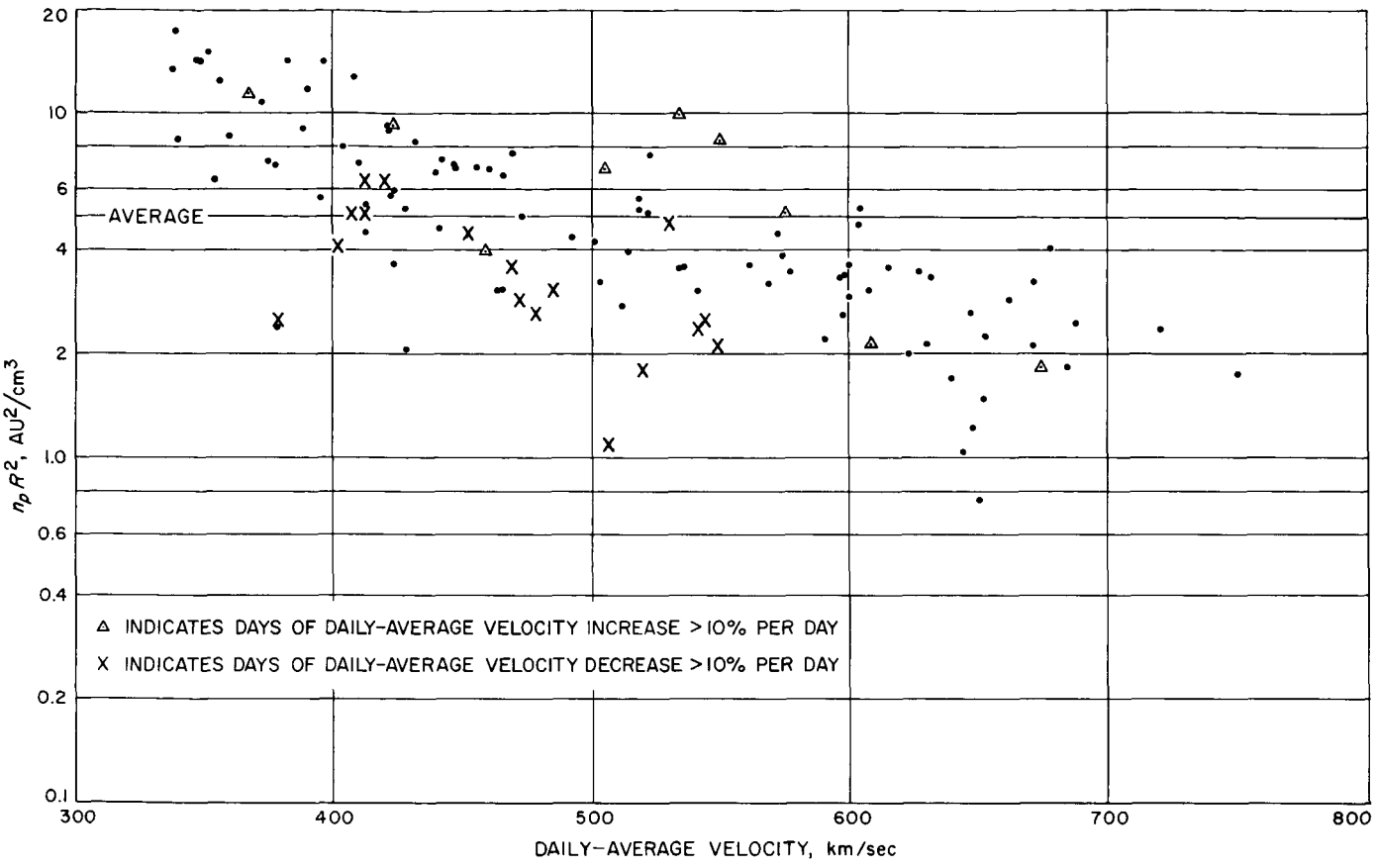

Fig. 7. Daily average of n_pR^2 vs. the daily average of v

velocity could never have been very different from radial, because no currents would have been observed at all for a net velocity (solar wind plus spacecraft) more than ~ 10 deg from the solar direction. However, smaller transverse velocity components that would significantly affect the density calculations cannot be ruled out. The present calculations, for example, would underestimate the true proton density on the leading edge of a high-velocity stream if the type of refraction discussed by Davis (Ref. 14) were significant. Furthermore, any tangential velocity component deriving from the probable corotation of the plasma close to the Sun would tend to cancel out the effect of the spacecraft motion, and the densities presented here would be higher than the true densities.

According to E. F. Lyon[4], the direction of the velocity vector (determined to an accuracy of a few degrees) was consistent with a radial flow for about 90% of *IMP-1*'s period of observation of the solar wind. Therefore, the calculations of long-time averages of proton density and the general trends of the density's temporal variations are probably reliable, although undetectable errors may have been present about 10% of the time.

The calculated values of proton density were also based on the assumption of an isotropic velocity distribution in the reference frame that moved with the plasma. If, for an extreme example, there were no thermal motion at all in the transverse directions, the calculated densities presented here should be decreased by a factor of 1.5 to 2.

C. Temperature

The upper and lower limits of the 3-hr averages of the proton temperature are shown in Fig. 9 where the time base was chosen to show the 27-day recurrence features associated with solar rotation. This plot of temperature vs. time generally follows the plot of bulk velocity vs. time (i.e., the high-velocity streams were hotter than the surrounding plasma).

[4]Unpublished communication at European Space Research Institute Conference, May 1966.

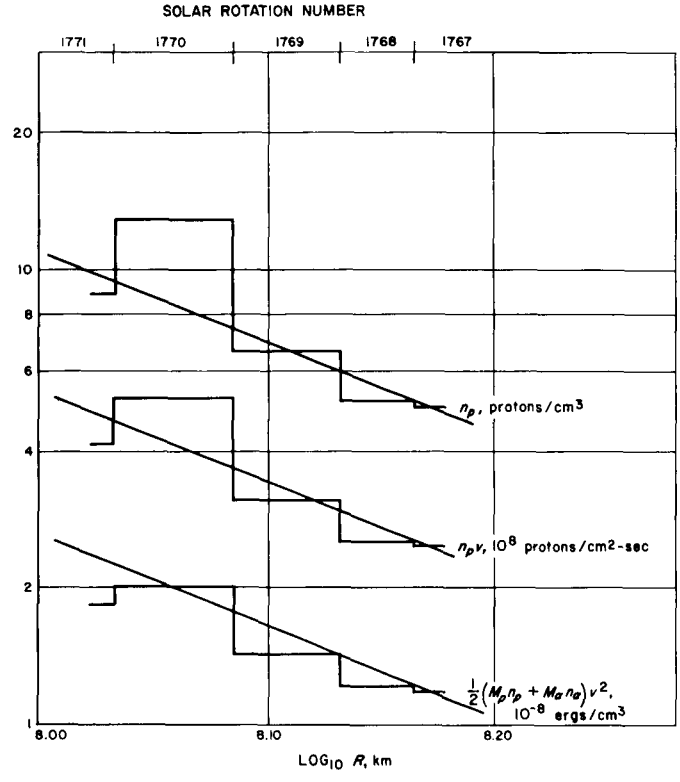

Fig. 8. Twenty-seven-day averages of the daily averages of n_p, $n_p v$, and $v^2 (M_p n_p + M_\alpha n_\alpha)/2$ vs. distance from the Sun

As a high-velocity stream overtook the spacecraft, the temperature usually increased more rapidly than did the velocity, and reached its maximum value several hours to half a day before maximum velocity was reached (examples are shown in Fig. 9 for September 12, September 19, October 7 and November 29).

The 3-hr averages of proton temperature ranged up to 8.0×10^5 °K on October 26. The highest temperature observed for at least three consecutive spectra was between 9.0 and 9.1×10^5 °K maintained for three spectra on December 17.

The average daily-average value of T_p for the entire experiment was between 1.51 and 1.85×10^5 °K (lower and upper limits). Thus the temperature of the interplanetary protons was, on the average, about a factor of 10 lower than the temperature at the base of the corona, and, occasionally, between the high-velocity streams, was cooler than the corona by a factor of about 50.

The 27-day averages of the daily averages of the upper and lower limits of T_p are plotted vs. distance from the Sun in Fig. 6. There was no obvious radial dependence. This conclusion is further verified by noting that the 3-hr temperature averages reached about the same minimum values of $\sim 3 \times 10^4$ °K for each of the between-stream periods found on the basis of bulk velocity.

Scarf's calculations of a model quiet solar wind based on assumptions of thermal conduction and viscous flow followed by adiabatic expansion[5] predict a temperature of 2.2×10^4 °K at 1 AU, while Sturrock and Hartle's two-fluid model of the solar wind (Ref. 10) predicts a positive-ion temperature of 2800 °K at 1 AU. These minimum temperatures correspond to the absence of any plasma heating by interactions with magnetic or electric-field fluctuations. Hence the observations of temperature by *Mariner II* may be evidence for appreciable heating of positive ions in the solar wind by field-particle interactions.

The ratio of proton thermal-energy to flow-energy densities,

$$3\theta_p/2 = (3kT_p/2)/(M_p v^2/2)$$

has also been studied. Figure 10 is a plot of the daily averages of the upper and lower limits of $3\theta_p/2$ vs. the daily-average velocity; the dependence on the time derivative of v is apparently more important than any dependence on velocity v. This behavior is probably understandable in terms of the instabilities, turbulence, and perhaps small shocks created at the leading edge of a stream when a high-velocity plasma overtakes the slower plasma in its path.

On December 17, the 3-hr averages of $3\theta_p/2$ reached a maximum of 0.053, while the maximum value maintained for at least three consecutive spectra was between 0.104 and 0.115. The actual minimum values of $3\theta_p/2$ could not be determined with this instrumentation.

The averages of the daily-average values of the lower and upper limits of $3\theta_p/2$ for the entire flight were 0.013 and 0.017, respectively. The 27-day averages of $3\theta_p/2$ are shown in Fig. 6.

The energy density of proton random motions was never more than a small fraction of the energy density of bulk motion. Preliminary comparisons of the *Mariner II* plasma and magnetic-field data indicate that the energy

[5]Personal communication, 1965.

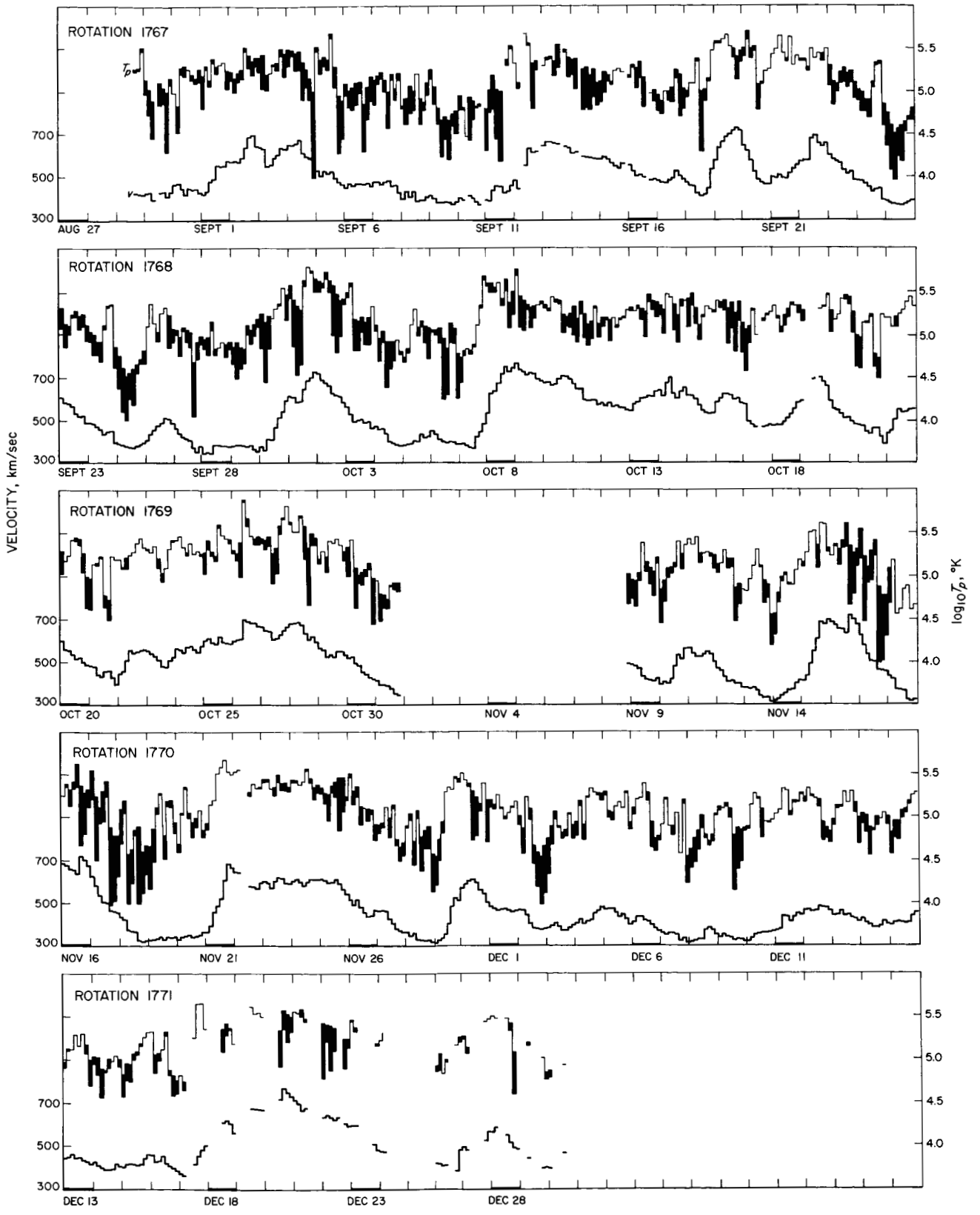

Fig. 9. Three-hr average values of v and T_p (logarithmic scale) vs. time (temperature limits have not been drawn below 10^4°K)

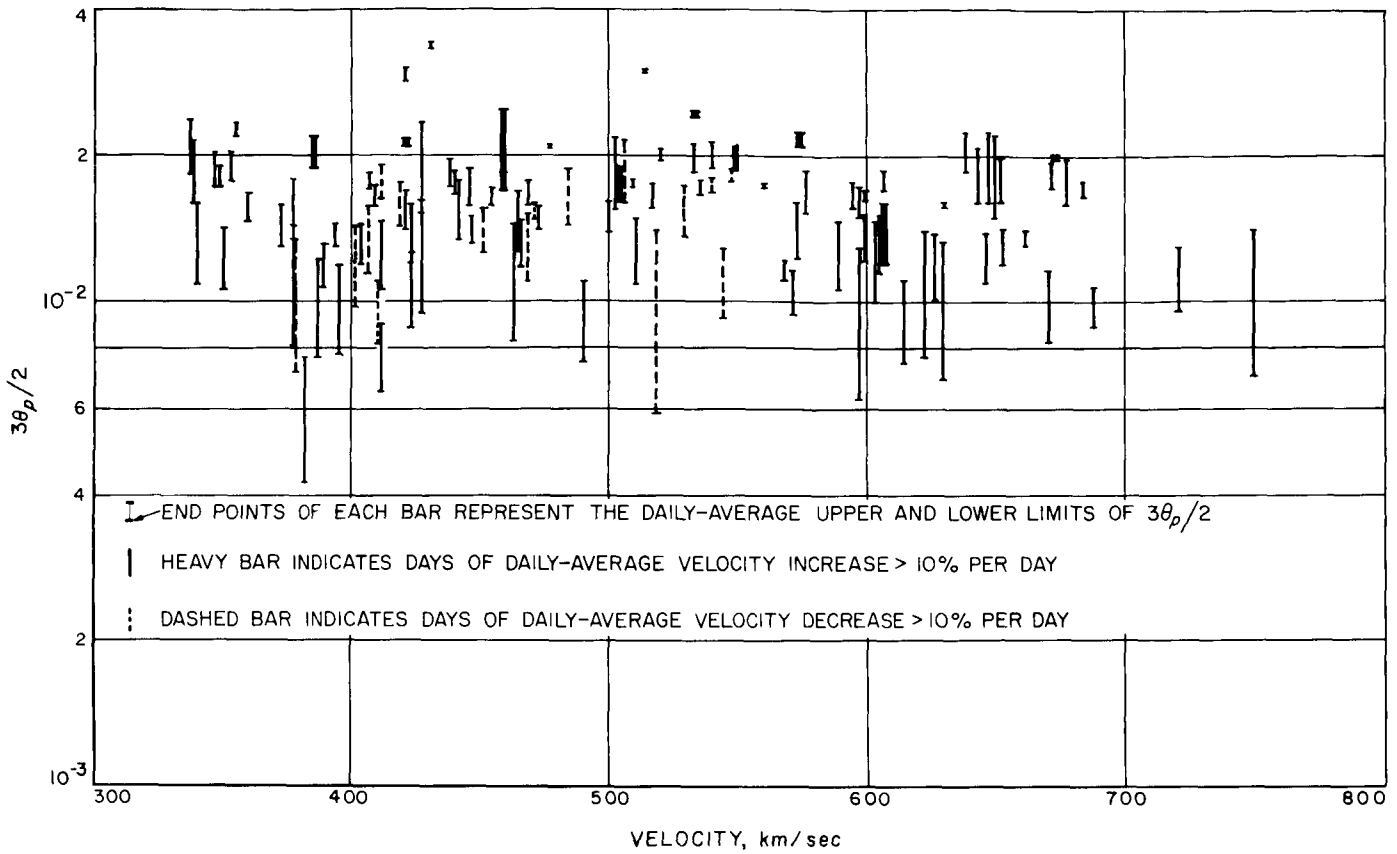

Fig. 10. Daily-average value of the ratio $3\theta_p/2$ vs. the daily-average solar-wind velocity

density of the interplanetary magnetic field was generally comparable to the thermal-motion energy density (Ref. 15). Thus, for problems involving only the momentum flux or energy density of the solar wind, use of the bulk-motion energy density alone would be a fair approximation; the electron energy density is probably not large (Ref. 16).

D. The Definition of T_p

Whether the parameters T_p and θ_p calculated from the spread in radial velocity are properly called temperature and a measure of thermal motions is questionable. The possibility that the observed velocity spread was really due to superposition of small, true, thermal motions on quite large, turbulent wave motion or other collective motions cannot be ruled out.

It is possible, however, to put an upper limit on the wavelength or scale size of any collective motions present. Because the electrometer time constant at the spectral peak was approximately 0.1 sec, and because the current in a given channel usually changed little, if at all, from one spectrum to the next, there could not have been any large amplitude motions present that changed appreciably over the distance swept out by the spacecraft in 0.1 sec in a reference frame moving with the solar wind. The limiting wavelength or scale size is thus approximately 50 km for an average solar wind of 500 km/sec. If, for example, the calculated T_p actually represented Alfvén waves moving through a fairly cold plasma at a velocity of V_A, the frequency of these Alfvén waves would have been greater than $V_A/50$ km. For $n_p = 5/\text{cm}^3$ and an interplanetary field strength of 5×10^{-5} gauss, V_A is about 50 km/sec; the wave frequency, then, must have been greater than $\sim$ 1 cps.

A better fit to the measured spectra can be obtained by assuming that the alpha particles had the same thermal velocity, rather than the same temperature, as the protons; this fact has at least two possible interpretations:

1. Collective motions were not of major importance, and the temperature of each type of ion was determined by such an ion-field interaction as reflections

from shock fronts moving through the plasma. (Ion-field interactions are expected to play an important role because the proton self-collision mean free path (Ref. 17) for a plasma with $T_p = 1.85 \times 10^5$ °K and $n_p = 5/\text{cm}^3$ is 2.7 AU.)

2. The velocity distributions were due to such motions as those found in transverse hydromagnetic (Alfvén) waves, in which the protons and alpha particles moved with a magnetic-field line, and therefore had the same velocities.

From a study of the correlations of plasma velocity and magnetic field observed by *Mariner II*, P. J. Coleman, Jr.,[6] found that the ratio of the power in velocity fluctuations to the power in magnetic-field fluctuations was independent of frequency in the range 1 to 116 cycles/day. On the basis of observations by *Mariner IV* and *OGO*, Coleman then extrapolated the magnetic-fluctuation spectrum to higher frequencies, and assumed that this ratio of powers remained constant at these higher frequencies; he found that the rms velocity for all oscillations with a frequency greater than 116 cycles/day was 4 km/sec. Because the thermal velocity was an order of magnitude greater than 4 km/sec, a temperature due to collective motions must have been the result of motions in which the magnetic field did not participate.

There are several possible sources of collective motions in the interplanetary medium:

1. Turbulent flow might be expected on the basis of the Reynolds number $nM_p vD/\mu$, (where D = scale size $\approx 10^{13}$ cm, and μ = viscosity $\approx 1.2 \times 10^{-16} T^{5/2}$ gm/cm sec), the value of which is about 10^3 in the relatively cool, dense plasma between streams. However, because the upper limit of the eddy sizes under consideration ($\sim$ 50 km) is 10^7 times less than the mean free path, and is approximately equal to the proton gyro radius for a thermal proton in the moving reference frame, it is not clear that the ordinary Reynolds number is a useful parameter.

2. Because the mean free path at 1 AU is so very large, because only the two degrees of thermal motion perpendicular to the radial direction are cooled by adiabatic expansion, and because collisions are too infrequent to restore isotropy, an anisotropic thermal velocity distribution might be expected. This anisotropic pressure could lead to either the hose or the mirror instability, depending upon the direction and strength of the interplanetary magnetic field (Ref. 18).

3. Both the two-stream and Kelvin-Helmholtz instabilities (Ref. 19), and collision-free shocks might be generated on the leading (western) edge of the high-velocity streams where hot, high-velocity plasma overtakes cooler, slower gas. At least one example of such a shock was observed by *Mariner II* (Ref. 8); the observable (low frequency) fluctuations in both the magnetic field and plasma were greatly enhanced behind this shock. The *Mariner II* data have also shown that these lower-frequency fluctuations, as exhibited by the standard deviations in velocity and the magnetic field (Ref. 20), were generally increased at the leading edges of the high-velocity streams.

Thus, because it seems likely that turbulent or wave motions would be generated in the interplanetary plasma, the answer to the question of whether T_p was primarily a measure of thermal or of collective motions depends on both the rate of creation of these disturbances, and on the rate of their dissipation into thermal energy through field-particle interactions. In either case, it is probably true that the values of T_p observed between 0.7 and 1.0 AU often depended in large part on disturbances generated in or propagating through the interplanetary medium, rather than on thermal conduction from the inner corona alone.

E. Nonthermal Ions

The parameter h was defined as $\log_{10}$ [I_{m+3} (measured)/I_{m+3} (calculated)]. A positive value of h therefore implies the presence of more ions with a large value of E/Q than predicted by a fit of Maxwell-Boltzmann distributions of protons and alpha particles (where $T_a = 4T_p$) to the currents measured in channels $m-1$, m, $m+1$, and $m+2$. If the possible contributions of any ions with mass/charge ratios greater than that for alpha particles are ignored, h can be considered a measure of any high-energy tail on the proton and alpha-particle distribution functions. It is only a semiquantitative measure of such a tail, however, because the ratio of measured to calculated currents was taken not at a fixed value of E/Q relative to the peak of the distribution function, but at a value of E/Q equal to 3.30 times the value of E/Q at the center of the channel with the largest current. Furthermore, it was not possible to separate the relative contributions of protons and alpha particles to the apparent tail.

[6]Personal communication, 1966.

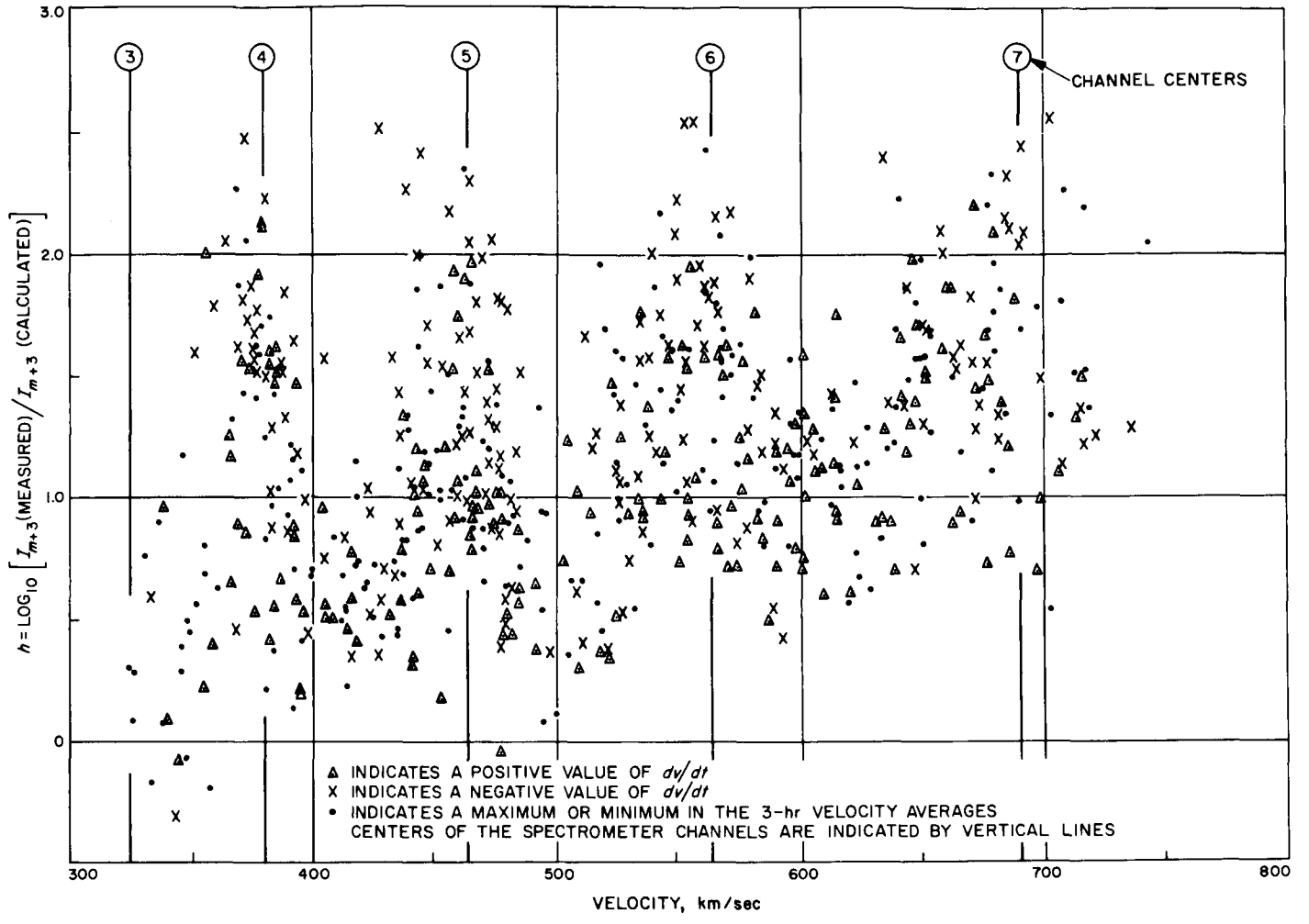

Fig. 11. Three-hr averages of the high-energy-tail parameter h vs. the 3-hr averages of plasma flow velocity

Figure 11 shows the distribution of 3-hr averages of h with the 3-hr averages of plasma velocity. The values of h showed some velocity dependence; in general, the high-energy tail was more pronounced when the velocity was high rather than low. Figure 11 also shows that h occasionally reached fairly high positive values, corresponding to about 300 times the expected current in channel $m+3$. The fact that h was seldom negative (except at velocities less than $\sim$ 360 km/sec) can be interpreted as evidence that an excess of high-energy ions was almost always present. The observation of a high-energy tail is in agreement with observations of the solar wind by *IMP-2* and *Vela 2A* (Ref. 21).

A significant high-energy tail often developed suddenly during the rising-velocity phase of a stream and then disappeared very slowly. For example, three consecutive spectra observed about 3 hr after the shock front seen on October 7 (Ref. 8) are shown in Fig. 12, where the dashed curves represent a rough fit of the proton and alpha-particle spectra to the currents in channels 4 through 7. There had been no current observed in channel $m+3$ for about 8½ hr preceding this time, and, after this time, large values of h were observed almost continuously for about a week. (Frame 63:115 shows one of the very few 7-point spectra obtained.) The sudden increase in h shown in Fig. 12 coincided with a change in direction of the interplanetary magnetic field of close to 180 deg. Some details of such correlations will be discussed in a later paper.

According to Fig. 11, h was generally greater on the trailing edge (negative dv/dt) than on the leading edge (positive dv/dt) of a high-velocity stream. The sudden appearance of a high-energy tail on the leading edge followed by the tail's slow decay (often over many days)

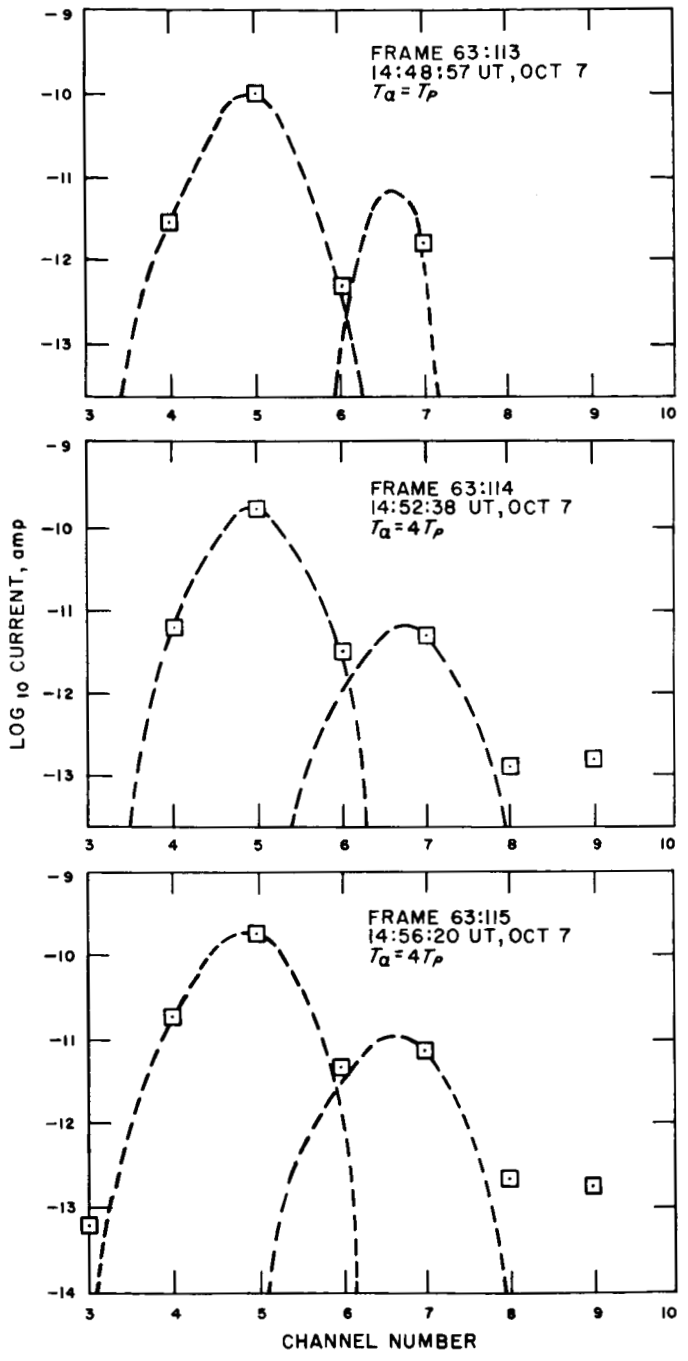

Fig. 12. Three consecutive positive-ion spectra obtained on October 7, 1962

is partially responsible for this effect. Also, larger values of h on the trailing edge of a stream often occurred in regions of low proton temperature and low values of I_{m+3} (calculated), rather than in regions of unusually high values of I_{m+3} (measured) similar to that shown in Fig. 11.

In Fig. 11, the quasi-periodic structure in phase with the spacing of the spectrometer channels probably arose from a combination of three effects:

1. As the proton peak occurred at higher values of E/Q relative to the center of channel m, the measurement of h was made at values of E/Q closer to the alpha-particle peak, where the fractional deviation from a Maxwell-Boltzmann distribution was smaller.

2. As the proton peak occurred at lower values of E/Q relative to the center of channel m, the current in channel $m+3$ was more likely to be unmeasurably small so that h could not be calculated.

3. If the proton peak was far above (or far below) the center of channel m, an unmeasurably small current in channel $m-1$ (or $m+1$) was likely, preventing the calculation of h.

The 27-day averages of the daily averages of h are plotted vs. distance from the Sun in Fig. 6. The h plot looks very much like an exaggerated version of the v plot, except that a slight increase of h with increasing distance from the sun might be inferred. If this increase is real, it may be explained on the basis of an increase in the occurrence of acceleration mechanisms in shocks and neutral sheets as the velocity profiles of the streams steepen.

F. Alpha-Proton Ratio

The calculated ratio of alpha-particle density to proton density, n_α/n_p, is almost certainly in error for a spectrum with a large high-energy tail. Therefore, only those spectra for which $|h| \leq 0.3$ (i.e., for which the observed spectrum fit the assumed model within 3 digitization levels) have been included in this study of the ratio n_α/n_p. Of the 14,147 spectra for which a value of h could be calculated, only 1,213 (8.6%) fit the model to this extent. Figure 13 is a plot of the daily value of N_α/N_h vs. the daily-average velocity; N_α is the number of spectra with $|h| \leq 0.3$, and N_h is the number of spectra for which a value of h could be calculated. It is evident that most of the "good-fit" spectra were observed during periods of low plasma velocity. This relation is consistent with the dependence of h on velocity discussed in the previous section.

Figure 14 shows the daily-average values of n_α/n_p plotted vs. the daily-average velocity for those days on

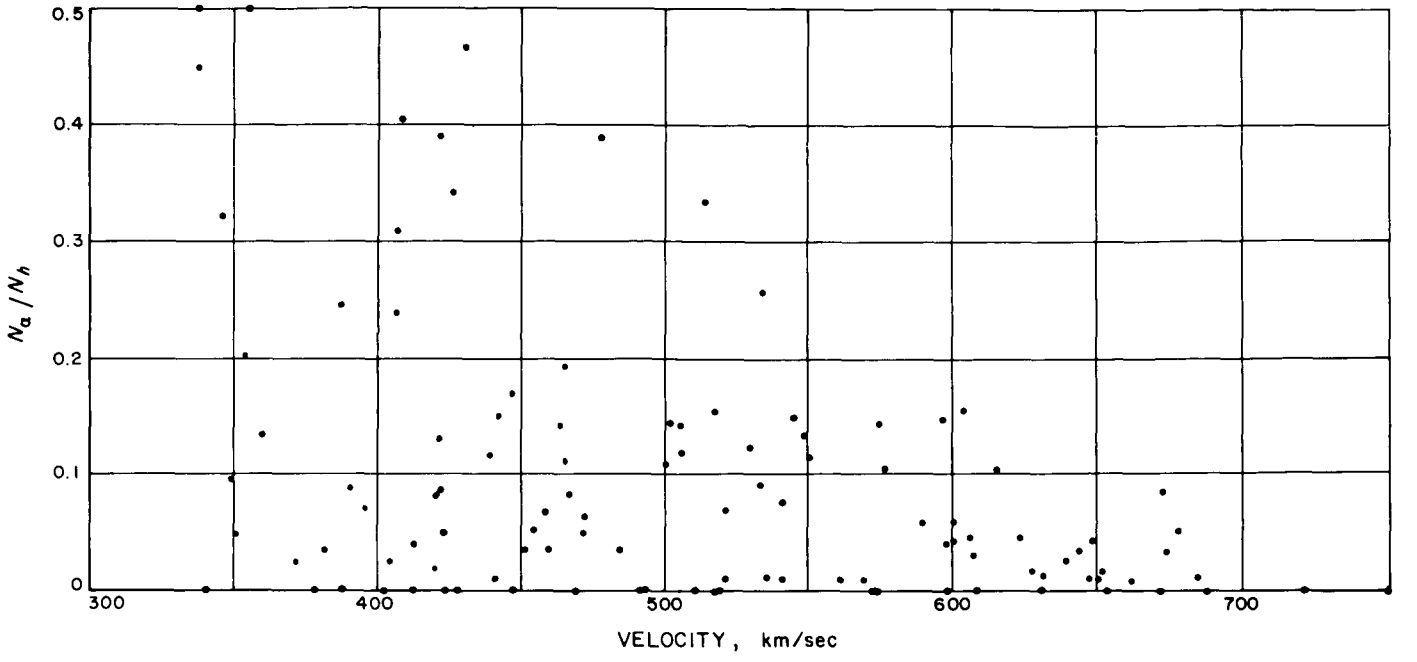

Fig. 13. Three-hr value of N_α/N_h vs. the 3-hr average solar-wind velocity

which $N_\alpha/N_h \geq 0.10$. There was no obvious dependence of n_α/n_p on either the velocity or its time derivative.

The average value and standard deviation of n_α/n_p for all the 1,213 spectra with $|h| \leq 0.3$ were 0.046 ± 0.038.

From a combination of spectroscopic and solar-cosmic-ray observations, Biswas and Fichtel (Ref. 22) determined the solar photospheric ratio of n_α/n_p to be ~ 0.09. The discrepancy between a solar ratio of 0.09 and the ratio observed by *Mariner II* may be due to the fact that the *Mariner II* values of n_α/n_p were heavily biased by low velocity conditions. A steady-state composition on the Sun could be maintained if greater amounts of helium were carried away from the Sun either in high-velocity streams, or in the plasma ejected from solar flares, or as solar cosmic rays.

The calculated values of n_α/n_p are strongly dependent on the underlying assumptions concerning the angle of incidence (assumed radial velocity), the relative alpha-particle and proton temperatures (assumed $T_\alpha = 4T_p$), and the relative alpha-particle and proton velocities (assumed $v_\alpha = v_p$). If a set of assumptions better than those used for this analysis result from future experiments of higher resolution, a recalculation of n_α/n_p from the *Mariner II* data using this set could give results quite different from those presented here.

Figure 15 is a plot of the mean value of n_α/n_p for each solar rotation vs. the logarithm of distance from the Sun. Because of the very large scatter about the mean values, it is not possible to reach any definite conclusions about the radial variation of the ratio n_α/n_p. However, since the general appearance of the spectra did not change between 1.0 and 0.7 AU, the ratio v_α/v_p (assumed = 1.00) could not have changed by as much as 20 or 30%. Because the quantity $(n_\alpha v_\alpha)/(n_p v_p)$ cannot be a function of distance from the Sun (assuming the same, if any, departure from a spherically symmetric flow for the two kinds of ion), it is unlikely that n_α/n_p changed by as much as 20 or 30% between 0.7 and 1.0 AU.

G. Persistence of High-Velocity Streams

The recurrent high-velocity streams discussed in this paper are probably earlier observations of the "quasi-stationary corotating structures" in Wilcox and Ness's analysis (Ref. 23) of *IMP-1* data. Besides magnetic-field data, Wilcox and Ness also presented their analysis of the solar-wind plasma data communicated to them by Lyon and Bridge. The *Mariner II* and *IMP-1* plasma experiments revealed similar relations between plasma velocity and the geomagnetic index K_p, and between plasma velocity and density; the density was a maximum about one day before the velocity peak, a minimum about

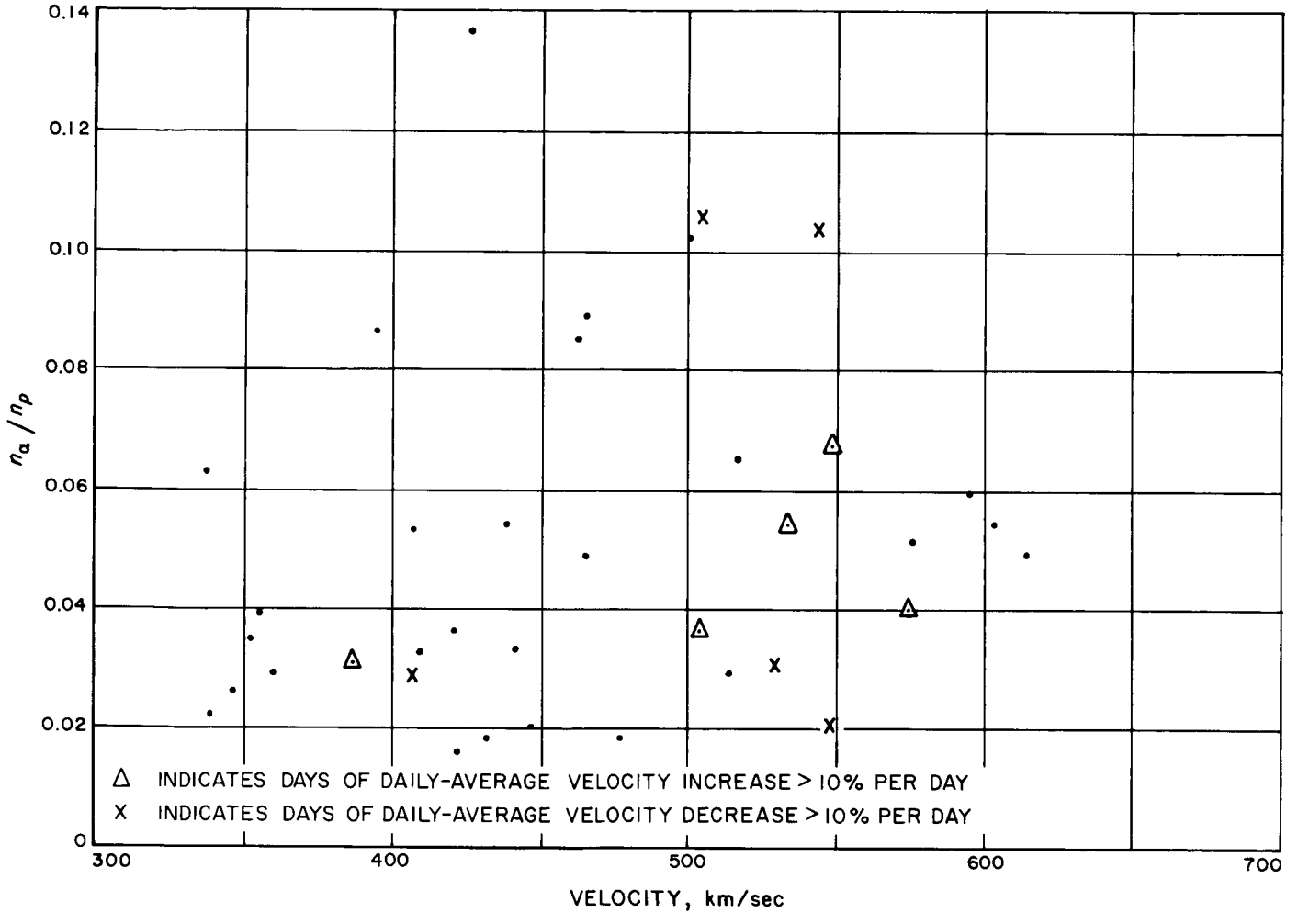

Fig. 14. Daily-average alpha-proton density ratio n_α/n_p vs. daily-average solar-wind velocity for those days on which $N_\alpha/N_h > 0.1$

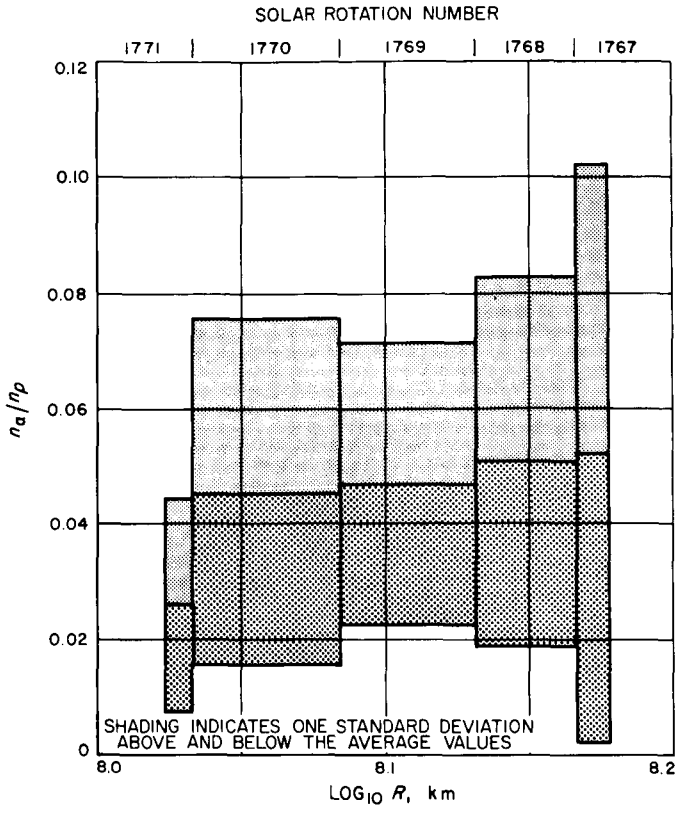

Fig. 15. Mean values of n_α/n_p for each solar rotation vs. the logarithm of distance from the Sun

two days after the velocity peak, and then increased while the velocity continued to decrease.

In particular, geomagnetic data indicate that the very long-lived *M*-region stream occurring roughly from the sixth through the twelfth days of each solar-rotation cycle was probably observed by both *Mariner II* (August–December, 1962) and *IMP-1* (November, 1963–February, 1964). Comparison of Wilcox and Ness's report (Ref. 23) with those of Davis, Smith, Coleman and Sonett (Ref. 20) and Coleman (Ref. 4) indicates that the interplanetary magnetic-field lines in this stream were pointing outward from the Sun during both the *Mariner* and *IMP* observations. Furthermore, Wilcox and Ness (Ref. 23) reported that Fan, Gloeckler, and Simpson's detector on *IMP-1* observed a recurrent counting-rate increase of protons with a few Mev of energy associated with this recurrent structure; Van Allen, Frank and Venkatesan (Ref. 24) reported particle fluxes above the galactic cosmic-ray background within a day of the peak velocity for each of the five appearances of this stream during the *Mariner II* experiment. Some of the particles observed by Van Allen, Frank, and Venkatesan could have been either protons with energy greater than 0.5 Mev, or electrons with energy greater than 40 kev; at other times, the particles could be identified as protons. Thus, although there were obvious changes in the detailed structure of this stream from one solar rotation to the next, many of its basic features were perhaps unchanged over a period of at least 18 months.

The other streams observed by *Mariner II* are probably the same kind of phenomenon as, but not the direct ancestors of the other quasi-stationary structures discussed by Wilcox and Ness (Ref. 23).

REFERENCES

1. Lincoln, J. V., "Solar and Geomagnetic Data," *J. Geophys. Res.*, vol. 67, pp. 5341–5342, 1962; vol. 68, pp. 581–585, 1155–1156, 1767–1768, and 2335–2342, 1963.

2. Neugebauer, M., and Snyder, C. W., "Solar-Wind Measurements Near Venus," *J. Geophys. Res.*, vol. 70, pp. 1587–1591, 1965.

3. Josias, C., and Lawrence, J. L., Jr., *An Instrument for Measurement of Interplanetary Solar Plasma*, Technical Report 32-492. Jet Propulsion Laboratory, Pasadena, Calif., May 1, 1964.

4. Coleman, P. J., Jr., *Irregularities in the Interplanetary Magnetic Field*, Ph.D. thesis. University of California, Los Angeles, Calif., 1966.

REFERENCES (Cont'd)

5. Snyder, C. W., Neugebauer, M., and Rao, U. R., "The Solar Wind Velocity and Its Correlation with Cosmic-Ray Variations and with Solar and Geomagnetic Activity," *J. Geophys. Res.*, vol. 68, pp. 6361–6370, 1963.

6. Snyder, C. W., and Neugebauer, M., "Interplanetary Solar-Wind Measurements by *Mariner* 2," *Space Res.*, vol. 4, pp. 89–113, 1964.

7. Maer, K., Jr., and Dessler, A. J., "Comment on the Paper by Conway W. Snyder et al., 'The Solar Wind Velocity and Its Correlation with Cosmic-Ray Variations and with Solar and Geomagnetic Activity,' " *J. Geophys. Res.*, vol. 69, p. 2846, 1964.

8. Sonnett, C. P., et al., "Evidence for a Collision-Free Magnetohydrodynamic Shock in Interplanetary Space," *Phys. Rev. Lett.*, vol. 13, pp. 153–156, 1964.

9. Scarf, F. L., *Lecture Notes on Plasma and Space Physics.* ASEE-NASA Summer Faculty Institute, 1965.

10. Sturrock, P. A., and Hartle, R. E., "Two-Fluid Model of the Solar Wind," *Phys. Rev. Lett.*, vol. 16, pp. 628–631, 1966.

11. Scarf, F. L., "The Origin of the Solar Wind," in *The Solar Wind*, pp. 199–212. Edited by R. J. Mackin, Jr., and Marcia Neugebauer. Jet Propulsion Laboratory, Pasadena, Calif. 1966. (Distributed through Pergamon Press, New York.)

12. Parker, E. N., "Dynamics of the Interplanetary Gas and Magnetic Fields," *Astrophys. J.*, vol. 128, pp. 664–676, 1958.

13. Parker, E. N., *Interplanetary Dynamical Processes.* Interscience Publishers, New York, 1963.

14. Davis, L., Jr., "Models of the Interplanetary Fields and Plasma Flow," in *The Solar Wind*, pp. 147–157. Edited by R. J. Mackin, Jr., and Marcia Neugebauer. Jet Propulsion Laboratory, Pasadena, Calif., 1966. (Distributed through Pergamon Press, New York.)

15. Neugebauer, M., and Snyder, C. W., "*Mariner*-2 Measurements of the Solar Wind," in *The Solar Wind*, pp. 3–21. Edited by R. J. Mackin, Jr., and Marcia Neugebauer. Jet Propulsion Laboratory, Pasadena, Calif., 1966. (Distributed through Pergamon Press, New York.)

16. Lyon, E. F., "*Explorer*-18 Plasma Measurements," in *The Solar Wind*, pp. 295–314. Edited by R. J. Mackin, Jr., and Marcia Neugebauer. Jet Propulsion Laboratory, Pasadena, Calif., 1966. (Distributed through Pergamon Press, New York.)

17. Spitzer, L., Jr., *Physics of Fully Ionized Gases*, Second Edition. Interscience Publishers, New York, 1962.

18. Parker, E. N., "Kinetic Properties of Interplanetary Matter," *Planetary Space Sci.*, vol. 9, pp. 461–475, 1962.

19. Dessler, A. J., and Fejer, J. A., "Interpretation of K_p Index and M-Region Geomagnetic Storms," *Planetary Space Sci.*, vol. 11, pp. 505–511, 1963.

20. Davis, L., Jr., et al., "Interplanetary Magnetic Measurements," in *The Solar Wind*, pp. 35–50. Edited by R. J. Mackin, Jr., and Marcia Neugebauer. Jet Propulsion Laboratory, Pasadena, Calif., 1966. (Distributed through Pergamon Press, New York.)

REFERENCES (Cont'd)

21. Wolfe, J. H., Silva, R. W., and Myers, M. A., "Preliminary Results from the Ames Research Center Plasma Probe Observations of the Solar-Wind—Geomagnetic Field interaction Region on Imp-II and OGO-I," *Space Research VI* (to be published).

22. Biswas, S., and Fichtel, C. E., "Nuclear Composition and Rigidity Spectra of Solar Cosmic Rays," *Astrophys. J.*, vol. 139, pp. 941–950, 1964.

23. Wilcox, J. M., and Ness, N. F., "Quasi-Stationary Corotating Structure in the Interplanetary Medium," *J. Geophys. Res.*, vol. 70, pp. 5793–5805, 1965.

24. Van Allen, J. A., Frank, L. A., and Venkatesan, D., "Small Solar Cosmic-Ray Events Observed with *Mariner* 2," *Trans. Am. Geophys. Union*, vol. 45, p. 80, 1964.

APPENDIX A

Method of Calculation of Plasma Parameters from Measured Spectra

I. VELOCITY AND TEMPERATURE

For a given spectrum, the peak channel, m, was usually the channel in which the largest current was observed. However, there were two exceptions to this general rule: (1) Because of the relatively wide spacing of the non-overlapping E/Q windows, the channel nearest the alpha-particle peak occasionally had a larger measured current than did any of the proton channels. Such occurrences were fairly obvious, and the appropriate proton channel could be easily selected as the peak channel. (2) If the actual proton peak was approximately midway between two adjacent spectrometer channels, these two channels had almost equal currents. When the currents in the two channels were within one digitization level (i.e., within a factor of $10^{0.1}$) of being equal, the channel at the lower value of E/Q was chosen to be the peak channel.

Let I_m denote the current in the peak channel, while I_{m-1} is the current in the adjacent channel at a lower value of E/Q. Similarly, I_{m+1} is the current in the channel just above the peak channel. The quantities R and Q are defined as follows:

$$R = \log_{10}(I_m/I_{m-1}) \tag{A-1}$$

$$Q = \log_{10}(I_m/I_{m+1}) \tag{A-2}$$

Figure A-1 shows the relation between R, Q, v, and θ for an isotropic Maxwell-Boltzmann distribution (in a reference frame moving radially away from the Sun with velocity v) for a single type of ion, where $v = v/v_m$ = plasma bulk velocity relative to the velocity at the center of the peak channel, and $\theta = 2kT/M_p v^2$. The dotted and lined areas in Fig. A-1 show the range of values of R and Q that correspond to selected values of v and θ, respectively, for a large range of values of angle of incidence.

The straight lines of constant v and constant θ in Fig. A-1 represent the following convenient set of approximations:

1. The average logarithmic value of the spacing of the channels was selected to make Fig. A-1 independent of the value of m.
2. The lines of constant v and constant θ were assumed to be independent of the angle between the normal to the detector aperture and the velocity vector of the plasma bulk motion.
3. The lines of constant θ can be represented by the equation:

$$\theta = 0.03026\,(R + 0.608Q)^{-1.194}. \tag{A-3}$$

4. The lines of constant v can be represented by the equation:

$$g(v) = (R - 0.3)/(Q + 0.3), \tag{A-4}$$

where the function $g(v)$ is shown in Fig. A-2.

The size of the errors in v and θ resulting from the use of the approximations given in listings 2, 3, and 4 above can be estimated from the differences between the straight lines and the shaded areas in Fig. A-1. Each of these four approximations can be justified on the basis that errors arising from their use are usually less than, or of the same order as the uncertainties arising from the digitization of the current measurements. The effects of these quantization uncertainties are discussed in more detail in Appendix B.

The parameter P is defined by

$$P = \log_{10}(I_m/I_{m+2}) \tag{A-5}$$

and a set of relations similar to Eqs. (A-3) and (A-4) can be found for $\theta(R,P)$ and $v(R,P)$. By elimination of θ between $\theta(R,Q)$ and $\theta(R,P)$, the following equation is obtained for the expected relation between R, Q, and P for a Maxwell-Boltzmann distribution of a single type of ion:

$$P = 6.44\,(R + 0.608Q)^{0.964} - 4.762R \tag{A-6}$$

The calculation of v and θ for a given spectrum proceeded as follows: for the first iteration, it was assumed that only protons contributed to the currents in channels $m-1$, m, and $m+1$; the measured values of I_{m-1}, I_m, and I_{m+1} were used to calculate R and Q from

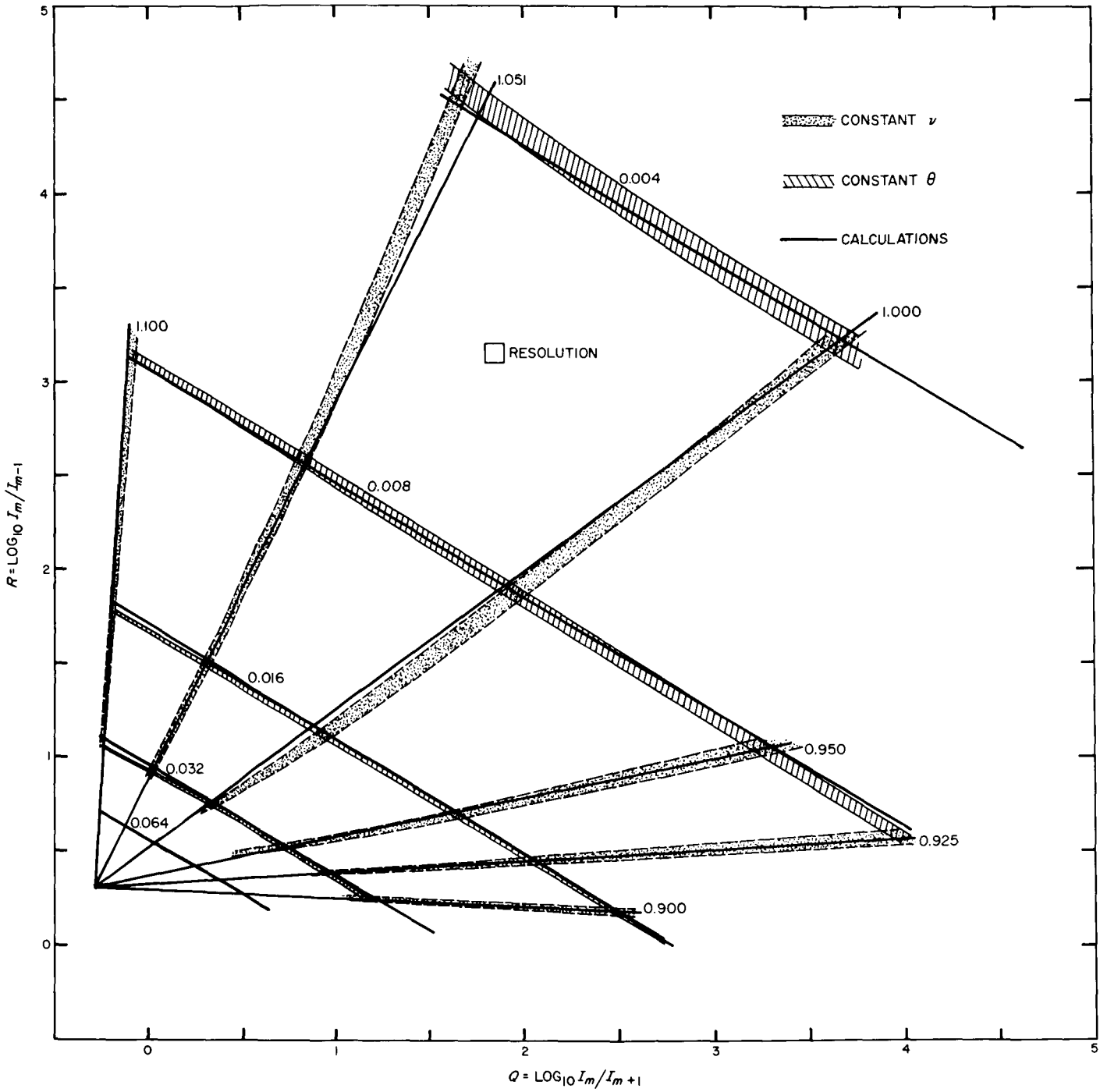

Fig. A-1. Contours of constant ν and constant θ as a function of the currents in channels $m-1$, m, and $m+1$ for a single type of ion

Eqs. (A-1) and (A-2); R and Q were used in Eqs. (A-3) and (A-4) to obtain first approximations to ν and θ; P was determined from Eq. (A-6). Then, according to Eq. (A-5), the proton contribution to the current in channel $m+2$ was $I_m \times 10^{-P}$; the remainder of the current in channel $m+2$ was assumed due to alpha particles.

If $\nu \geq 0.947$, and if the alpha particles had the same bulk velocity as the protons, then the alpha-particle peak would have been nearest channel $m+2$; if the alpha-particles had the same thermal velocity as the protons, then the value of θ would have been the same for the two kinds of ions. If $r = \log_{10}(I^a_{m+2}/I^a_{m+1})$ and

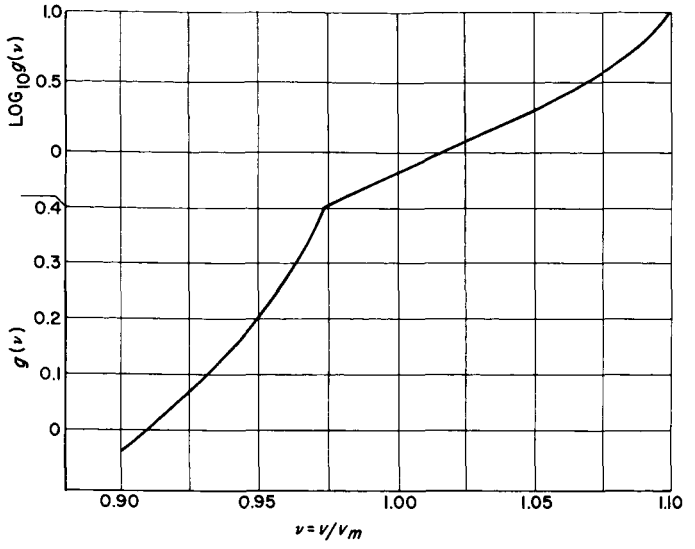

Fig. A-2. The function $g(v)$ vs. v

$q = \log_{10}(I^a_{m+2}/I^a_{m+3})$, where the superscript a refers to the alpha-particle contribution, then, from Eq. (A-3), the assumption that $\theta_a = \theta_p$ can be written in the form:

$$r + 0.608q = R + 0.608Q, \tag{A-7}$$

while Eq. (A-4) gives

$$g(0.950v) = (r - 0.3)/(q + 0.3) \tag{A-8}$$

The factor 0.950 in Eq. (A-8) is the ratio of the proton velocity at the center of channel m to the alpha-particle velocity at the center of channel $m+2$. Elimination of q from Eqs. (A-7) and (A-8) gives

$$r = \frac{g(0.950v)\,(R + 0.608Q + 0.1824) + 0.1824}{0.608 + g(0.950v)} \tag{A-9}$$

The alpha-particle contribution to the current in channel $m+1$ is then given by

$$I^a_{m+1} = I^a_{m+2} \times 10^{-r} = 10^{-r}(I_{m+2} - I_m \times 10^{-P}) \tag{A-10}$$

A correction can now be made to the assumption that only protons contributed to the current in channel $m+1$, and the whole calculation is repeated with a new value of Q:

$$Q' = \log_{10}[I_m/(I_{m+1} - I^a_{m+1})]$$

The iteration is considered to be sufficiently converged when successive values of Q agree within a factor of $10^{0.03}$ (i.e., within 0.3 digitization levels). For some of the *Mariner II* spectra, the iteration does not converge before I^a_{m+1} becomes greater than I_{m+1}. For many of these spectra, however, convergence can be obtained if one assumes that the protons and alpha particles had equal temperatures rather than equal thermal velocities. In this case, $\theta_a = \theta_p/4$, and the procedure for finding v and θ is similar to that outlined above.

If $v < 0.947$, the equations used must be modified slightly because the alpha-particle peak is nearer channel $m+1$ than channel $m+2$. Specifically, for the equal-thermal-velocity model, r is eliminated between Eq. (A-7) and an equation similar to Eq. (A-8) to obtain

$$q \equiv \log_{10}(I^a_{m+1}/I^a_{m+2})$$

$$q = \frac{R + 0.608Q - 0.3 - 0.3g(1.159v)}{0.608 + g(1.159v)} \tag{A-11}$$

where, in this case, 1.159 is the ratio $v_{m,p}/v_{m+2,a}$. Then the correction to be subtracted from I_{m+1} is

$$I^a_{m+1} = I^a_{m+2} \times 10^q = (I_{m+2} - I_m \times 10^{-P})10^q \tag{A-12}$$

The velocity must be corrected for the radial component (v_r) of the spacecraft's velocity to obtain the plasma velocity relative to the sun, v_o:

$$v_o = v\,v_m + v_r \tag{A-13}$$

During the course of the *Mariner II* mission, v_r changed from $-$ 1.2 to $-$ 6.3 to + 0.7 km/sec.

The proton temperature is given by:

$$T_p(^\circ\mathrm{K}) = 60.57\,v^2 v_m^2 \theta_p \tag{A-14}$$

for v_m in units of km/sec.

II. PROTON DENSITY

Although the shape of the observed spectrum, and therefore the calculated values of the plasma's velocity and temperature, is relatively insensitive to the angle of incidence of the plasma flow, the absolute values of the measured currents, and therefore of both the plasma density and flux, are very sensitive to direction. If we assume that the plasma flows radially away from the Sun, then the angle of incidence on the spectrometer aperture is a known function of the spacecraft's velocity, of the spacecraft's orientation in space, and of the plasma velocity calculated in the previous section.

Since the spectrometer's aperture always faced the Sun, a coordinate system is defined in which the z axis is radially away from the Sun and parallel to the aperture's normal. The x and y axes are chosen so that the xz plane is the analysis plane (Fig. A-3). Then, according to the model chosen (i.e., an isotropic Maxwell-Boltzmann distribution at temperature T in a coordinate system moving radially away from the Sun with velocity v), the current measured in channel j is related to the properties of the plasma, to the spacecraft's trajectory, and to the spectrometer's transmission function by the equation:

$$I_m = QA \iiint \delta(w_y, w_z)\, \varepsilon(w_x, w_z)\, (v + w_z) \quad n\left(\frac{M}{2\pi kT}\right)^{3/2} \exp[-M(w_x^2 + w_y^2 + w_z^2)/2kT]\, dw_x dw_y dw_z \qquad \text{(A-15)}$$

where Q is the charge on each ion (considering, now, only a single type of ion), A is the aperture area (5.0 cm^2), δ is the transmission function (or transparency factor) in the yz plane, and ε is the transmission function in the xz plane.

The transverse transmission function δ can be written as:

$$\delta = 0 \qquad \text{for } w_y \leq -v_{sy} - \frac{v + w_z}{5.69}$$

$$\delta = 1 + \frac{5.69\,(v_{sy} + w_y)}{v + w_z} \qquad \text{for } -v_{sy} - \frac{v + w_z}{5.69} \leq w_y \leq -v_{sy}$$

$$\delta = 1 - \frac{5.69\,(v_{sy} + w_y)}{v + w_z} \qquad \text{for } -v_{sy} \leq w_y \leq -v_{sy} + \frac{v + w_z}{5.69}$$

$$\delta = 0 \qquad \text{for } -v_{sy} + \frac{v + w_z}{5.69} \leq w_y$$

where v_{sy} is the y component of the spacecraft's velocity, v_s.

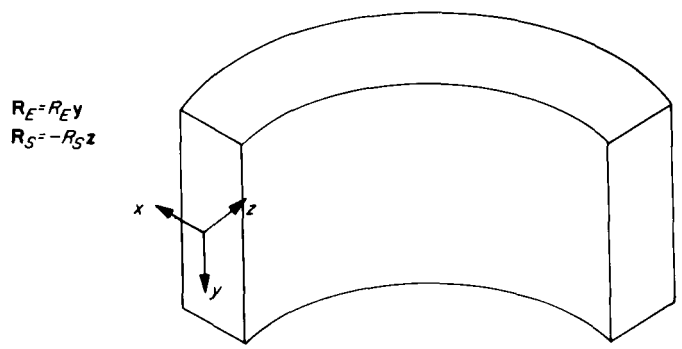

Fig. A-3 Coordinate system used in data analysis

The variation of ε with energy and angle of incidence in the analysis plane is shown in Fig. 3. The w_y integration in Eq. (A-15) can be done analytically, and the other two integrations have been done numerically to obtain a simplified form for Eq. (A-15):

$$I_j = QAnvv_j f(\phi, s, \theta, v) \qquad \text{(A-16)}$$

where ϕ is the roll angle, given in Table 1, and $s = v_{sxy}/v_j$, the component of the spacecraft's velocity in the xy plane relative to the ion velocity at the center of channel j.

The function $f(\phi, s, \theta, v)$ is illustrated in Fig. A-4 for the case $\phi = 30°$, $s = 0.0755$, and in Fig. A-5 for the case $\phi = 30°$, $\theta = 0.008$. Since the dimensions of the analyzer were chosen so that the angular apertures in the xz and the yz planes were approximately equal, $f(\phi, s, \theta, v)$ is not very sensitive to variations in ϕ. In fact, no correlation has been found between the calculated plasma properties and the angle ϕ during the six days that the spacecraft rolled about the probe–Sun vector. Figure A-1 and Eqs. (A-3) and (A-4) were derived by using sets of figures such as Figs. A-4 and A-5.

The proton density n_p is found from the measured spectra by rewriting Eq. (A-16) in the form:

$$n_p = \frac{I_m \times 10^{-14}}{8v\, v_m f(\phi, s, \theta, v)} \text{ (cm}^{-3}\text{)} \qquad \text{(A-17)}$$

for I_m, the current in the peak channel, in amp, and v_m in km/sec. The value of $f(\phi, s, \theta, v)$ was computed by first rounding off the actual value of ϕ to the nearest 15° and then performing a three-dimensional, logarithmic interpolation for the dependent variables s, θ, and v.

III. ALPHA-PROTON DENSITY RATIO

Equation (A-16) can be written for the alpha-particle current in channel $m+2$, the proton current in channel $m+2$, and the proton current ($\approx$ the total current) in channel m, respectively, as:

$$I^{a}_{m+2} = 2QAvn_{a}f\,(\phi, 0.950s, \theta, 0.950v)$$

$$I^{p}_{m+2} = QAvn_{p}f\,(\phi, 0.674s, \theta, 0.674v) = I_{m+2} - I^{a}_{m+2}$$

$$I_{m} = QAvn_{p}f\,(\phi, s, \theta, v)$$

These equations can be combined to yield:

$$n_{a}/n_{p} = \frac{f(\phi, s, \theta, v,)\,(I_{m+2}/I_{m}) - f(\phi, 0.674s, \theta, 0.674v)}{2f(\phi, 0.950s, \theta, 0.950v)} \tag{A-18}$$

Equation (A-18) is for the equal-thermal-velocity model in which the value of θ is the same for the protons and alpha particles. If a spectrum fits an equal-temperature model better, then equation Eq. (A-18) should be modified to give:

$$n_{a}/n_{p} = \frac{f(\phi, s, \theta, v,)\,(I_{m+2}/I_{m}) - f(\phi, 0.674s, \theta, 0.674v)}{2f(\phi, 0.950s, \theta/4, 0.950v)} \tag{A-19}$$

where θ refers to the value for protons.

IV. SUPERTHERMAL-PARTICLE PARAMETER

The parameter h was defined as:

$$h = \log_{10}\frac{I_{m+3}\,(\text{measured})}{I_{m+3}\,(\text{calculated})}$$

It can be assumed that the proton contribution to the current in channel $m+3$ is negligible compared to the alpha-particle contribution.

If $v \geq 0.947$,

$$I_{m+3}\,(\text{calculated}) = I^{a}_{m+2}\,10^{-q} = (I_{m+2} - I_{m}10^{-P})\,10^{-q}$$

where, for the equal-thermal-velocity model,

$$q = \frac{(R + 0.608Q) - 0.3g(0.950v) - 0.3}{g(0.950v) + 0.608}$$

whereas, for the equal-temperature model,

$$q = \frac{3.193(R + 0.608Q) - 0.3g(0.950v) - 0.3}{g(0.950v) + 0.608}$$

If $v < 0.947$,

$$I_{m+3}\,(\text{calculated}) = (I_{m+2} - I_{m}10^{-P})10^{q-p}$$

where, for the equal-thermal-velocity model,

$$q = \frac{R + 0.608Q - 0.3g(1.159v) - 0.3}{g(1.159v) + 0.608}$$

$$p = 6.44(R + 0.608Q)^{0.964} - 4.762(R + 0.608Q) + 2.895q$$

whereas, for the equal-thermal-velocity model,

$$q = \frac{3.193(R + 0.608Q) - 0.3g(1.159v) - 0.3}{g(1.159v) + 0.608}$$

$$p = 19.73(R + 0.608Q)^{0.964} - 15.21(R + 0.608Q) + 2.895q$$

The final, iterated values of v and Q are used to calculate q and p from these equations.

APPENDIX B

Accuracy of Calculated Parameters

The principal approximations used in fitting the *Mariner II* plasma data to the chosen models were:

1. Digitization of current measurements: this is probably the most important source of uncertainty in the calculated parameters. The velocity depends on the ratio $(R - 0.3)/(Q + 0.3)$; R and Q are defined in Appendix A. For all the observed combinations of R and Q, the largest possible uncertainty in v *is* $\Delta v/v = 0.02$. For a typical spectrum with $\theta_p = 0.01$, $\Delta v/v \leq 0.007$. The digitization errors in the parameters θ_p, n_p, and n_a/n_p are shown as functions of θ_p in Fig. B-1. The curves in this figure correspond to the largest possible fractional uncertainty for most of the observed spectra for the equal-thermal-velocity model; it is possible, however, to find spectra for which certain combinations of one-half-step perturbations make the difference, especially at large values of θ_p, between convergence or lack of convergence of the iterative calculation. Because the fractional error in velocity is small, $\Delta T_p/T_p \approx \Delta\theta_p/\theta_p$, $\Delta(n_p m_p v^2)/(n_p m_p v^2) \approx \Delta n_p/n_p$, etc.

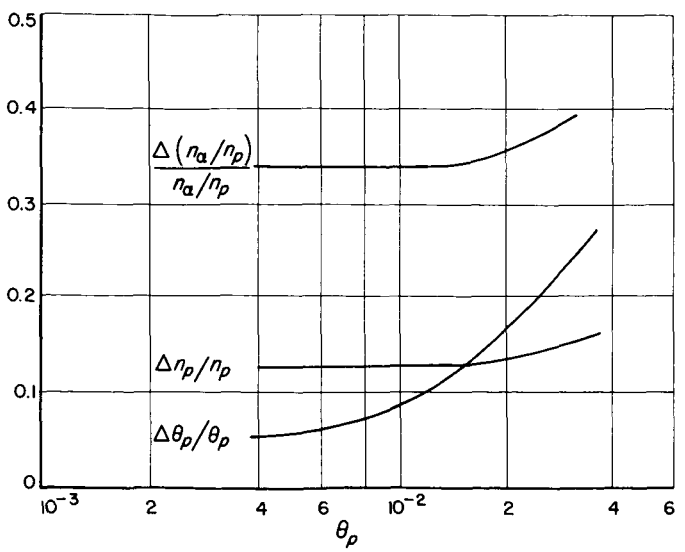

Fig. B-1. The largest possible fractional uncertainties in θ_p, n_p, and n_a/n_p arising from the 0.1-decade digitization of the current measurements

2. Spacing of E/Q channels: the ratio v_{m+1}/v_m ranged from 1.207 to 1.228. A value of 1.220 was assumed for this analysis, resulting in velocity errors of 1% or less. The resultant percentage errors in θ_p, n_p, n_a/n_p, etc., are much smaller than the percentage uncertainties due to the digitization of the current measurements.

3. Edge effects, scattering of ions, etc., neglected in calculation of the transmission function: the theoretical transmission function used for this analysis (Fig. 3) was based on the assumption of a purely radial electric field with absorption or neutralization of all ions that hit the analyzer electrodes. Figure B-2 compares the curves of constant ν and constant θ of this assumed transmission function with similar curves for the extreme case of a square transmission function for which:

$$\delta = 1 \text{ if } -0.15 \leq \frac{w_y}{v_m} \leq +0.15; \text{ otherwise, } \delta = 0$$

$\varepsilon = \alpha\beta$, where

$$\alpha = 1 \text{ if } -0.15 \leq \frac{w_x}{v_m} \leq +0.15; \text{ otherwise, } \alpha = 0$$

$$\beta = 1 \text{ if } 0.95 \leq \frac{v + w_z}{v_m} \leq 1.05; \text{ otherwise, } \beta = 0$$

For an average spectrum with $\theta_p \approx 0.01$, the error in the calculated values of ν and θ_p arising from the lack of a precise knowledge of the resolution function is probably no greater than the uncertainty arising from the digitization of the current measurements.

4. Spacecraft potential: in interplanetary space, the spacecraft potential is probably between zero and a few volts negative. A 10-volt potential would amount to a 2.5% shift in the effective velocity of channel 1, and a 0.06% shift in the velocity of channel 10. If the spacecraft had had a very large potential of either sign, the alpha-particle peak would

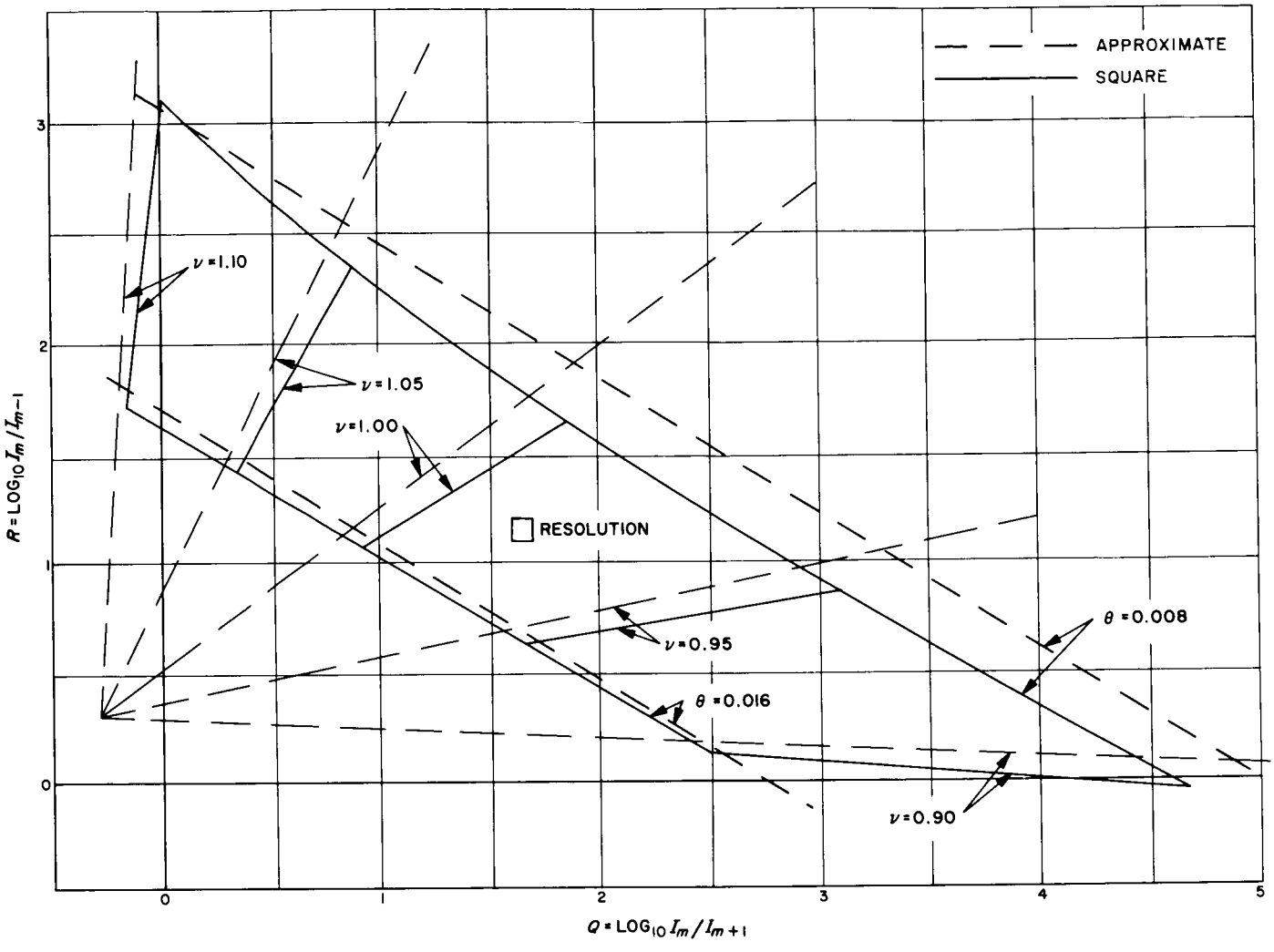

Fig. B-2. Contours of constant ν and constant θ as a function of the currents in channels $m-1$, m, and $m+1$ for an approximate and a square transmission function

not have been observed at a value of E/Q approximately twice that of the proton peak; spacecraft potential, therefore, was neglected.

5. Other approximations used, all of which gave errors less than the digitization uncertainties:

   a. ν and θ assumed independent of ϕ and s.

   b. ν and θ in simple relation to R, Q, and P.

   c. Quantization, rather than interpolation of ϕ, in calculation of n_p.

   d. Convergence of iteration considered satisfied when successive values of Q change by ≤ 0.03.

ACKNOWLEDGEMENT

The data analyzed in this Report could not have been obtained without the extraordinary efforts of C. Josias, J. Lawrence, Jr., and H. R. Mertz in designing, constructing, and testing the electronic equipment. We are also indebted to Kurt Heftman, Truman Cox, Patricia Conklin, and Margot Masin for their help in data handling and reduction.